AD-A165 593 GRATING INTERFEROMETRIC SENSORS(U) ENVIRONMENTAL RESEARCH INST OF MICHIGAN ANN ARBOR A M TAI FEB 86 ERIM-163700-12-F ARO-18491.6-PH DAAG29-82-K-0173 1/1

UNCLASSIFIED F/G 17/5 NL

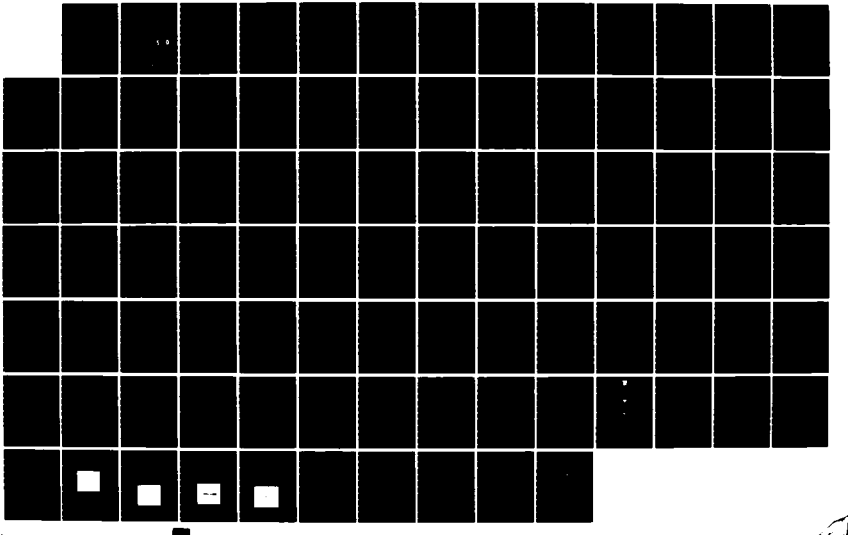

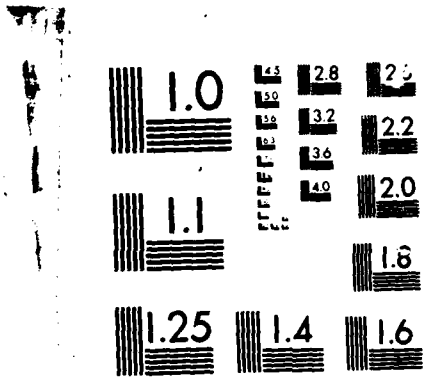

Final Technical Report

GRATING INTERFEROMETRIC SENSORS

ANTHONY M. TAI
Infrared and Optics Division

FEBRUARY 1986

U.S. Army Research Office
P.O. Box 12211
Research Triangle Park, NC 27709

ENVIRONMENTAL
RESEARCH INSTITUTE OF MICHIGAN
BOX 8618 • ANN ARBOR • MICHIGAN 48107

UNCLASSIFIED

SECURITY CLASSIFICATION OF THIS PAGE

AD-A165 593

REPORT DOCUMENTATION PAGE

1a. REPORT SECURITY CLASSIFICATION UNCLASSIFIED	1b. RESTRICTIVE MARKINGS
2a. SECURITY CLASSIFICATION AUTHORITY	3. DISTRIBUTION/AVAILABILITY OF REPORT
2b. DECLASSIFICATION/DOWNGRADING SCHEDULE	
4. PERFORMING ORGANIZATION REPORT NUMBER(S) 163700-12-F	5. MONITORING ORGANIZATION REPORT NUMBER(S)
6a. NAME OF PERFORMING ORGANIZATION Environmental Research Institute of Michigan 6b. OFFICE SYMBOL (If applicable)	7a. NAME OF MONITORING ORGANIZATION U.S. Army Research Office
6c. ADDRESS (City, State and ZIP Code) Infrared and Optics Division P.O. Box 8618 Ann Arbor, MI 48109	7b. ADDRESS (City, State and ZIP Code) P.O. Box 12211 Research Triangle Park, NC 27709
8a. NAME OF FUNDING/SPONSORING ORGANIZATION U.S. Army Research Office 8b. OFFICE SYMBOL (If applicable)	9. PROCUREMENT INSTRUMENT IDENTIFICATION NUMBER Contract DAAG29-82-K-0173
8c. ADDRESS (City, State and ZIP Code) P.O. Box 12211 Research Triangle Park, NC 27709	10. SOURCE OF FUNDING NOS. PROGRAM ELEMENT NO. / PROJECT NO. / TASK NO. / WORK UNIT NO.
11. TITLE (Include Security Classification) Grating Interferometric Sensors	
12. PERSONAL AUTHOR(S) Anthony M. Tai	
13a. TYPE OF REPORT Final Technical Rept 13b. TIME COVERED FROM 09/1/82 TO 10/31/85	14. DATE OF REPORT (Yr., Mo., Day) 15. PAGE COUNT
16. SUPPLEMENTARY NOTATION	
17. COSATI CODES FIELD / GROUP / SUB. GR	18. SUBJECT TERMS (Continue on reverse if necessary and identify by block number)

19. ABSTRACT (Continue on reverse if necessary and identify by block number)

A new class of grating-based interferometric sensors are introduced for target discrimination, detection and passive synthetic aperture imaging. It is shown that the grating-based interferometric sensors provides superior system sensitivity and flexibility. Several design approaches and operating modes of the grating interferometric sensors are presented and experiments demonstrating the proposed system concepts are described.

20. DISTRIBUTION/AVAILABILITY OF ABSTRACT UNCLASSIFIED/UNLIMITED ☐ SAME AS RPT ☐ DTIC USERS ☐	21. ABSTRACT SECURITY CLASSIFICATION UNCLASSIFIED
22a. NAME OF RESPONSIBLE INDIVIDUAL	22b. TELEPHONE NUMBER (Include Area Code) 22c. OFFICE SYMBOL

DD FORM 1473, 83 APR EDITION OF 1 JAN 73 IS OBSOLETE.

SECURITY CLASSIFICATION OF THIS PAGE

PREFACE

The work reported here was performed in the Electro-Optics Department of the Infrared and Optics Division, of the Environmental Research Institute of Michigan (ERIM). This work was sponsored by the U.S. Army Research office under Contract DAAG29-82-K-0173.

The report covered work performed between September 1, 1982 and October 31, 1985. The contract monitor was Dr. B. D. Guenther of the Army Research Office. The principal investigator was Anthony Tai. Major contributors to this effort were Anthony Tai, C. Aleksoff, K. Ellis, I. LaHaie, and N. Subotic.

CONTENTS

LIST OF FIGURES

GRATING INTERFEROMETRIC SENSORS

1
INTRODUCTION

Conventional remote sensing approaches provide information on the intensity distribution of the object scene with a resolution defined by the real collection aperture of the sensor. In this research project, we explored the use of coherence measurements to provide additional information that may help to enhance the capability of a remote sensor to discriminate between different targets or between targets and the background in the visible wavelengths. The enhancement can be accomplished by improving the image resolution beyond that permitted by the real collection aperture or by providing information beyond the intensity distribution of the object scene. In particular, the use a grating interferometer to perform the coherence measurements was examined.

It is useful to separate coherence measurements and their applications into two categories: 1) Measurement of the field coherence at the object plane where the object scene is under partially coherent illumination. 2) Measurement of the field coherence at the detection plane where the object scene is self emissive or under non-coherent illumination.

Measurement of the field coherence at the object plane can be performed by mapping the object field to the detection plane with an imaging system. We have shown that for an actively illuminated target, the image obtained through a scattering medium can be significantly enhanced by measuring the coherence of the image field with a grating interferometer and removing the contribution of the incoherent scattered light to the image intensity [1-3]. Coherence measurement at the object

plane can also be used to obtain additional information on a target scene. When partially coherent field is reflected by an object surface, its coherence properties may be altered by differing amounts, depending on the composition of the surface material and texture (surface height variations). Thus by measuring the coherence of reflected field, unresolved surface height variations may be inferred. Speckles, which are produced by mutual interference of adjacent pixels can be used to determine the coherence of the object field. It is well known that by illuminating a surface with partially coherent light whose longitudinal coherence length is of the same magnitude as the surface height variations, the texture of the object surface can be determined from the contrast of the image speckles [4,5]. Such a technique has been applied in metrology to study the surface texture of machined parts. The approach however, has not been applied to study the surface height variations over a large surface area for the purpose of target discrimination in a remote sensing system.

If the object field is self-emissive or under non-coherent illumination, the field at the object plane is simply incoherent, no useful information can be gained from measuring the coherence at the object plane. However, there is a Fourier transform relationship between the intensity distribution of the object scene and the spatial coherence at a distance detection plane. This relationship is utilized by a new class of passive sensors to achieve image resolution beyond the diffraction limits of their input apertures. The grating interferometer is capable of measuring the complex spatial coherence of an optical field very efficiently. We shall show in this report, how the grating interferometer may be used to detect the presence of moving targets and to perform passive synthetic aperture imaging.

While we have utilized the grating interferometer for object plane coherence measurements to achieve improve seeing through scattering medium and target discrimination [1-3], the same approach can also be implemented with conventional interferometers albeit less easily in some

cases. The grating interferometer however, offers some unique capabilities when used for coherence measurements at the detection plane to perform for example, synthetic aperture imaging. For this reason, we shall concentrate, in this report, on the use of the grating interferometer for detection plane coherence measurements.

In following sections, the van Cittert-Zernike theorem which forms the basis for passive interferometric imaging is first reviewed. The measurement of the mutual coherence function with a grating interferometer is then described and the possible uses of the interferometer for passive synthetic aperture imaging and as a moving target sensor are discussed. An overview of the grating interferometric sensors is given in the main body of the report. The operation of the grating interferometer and its uses in incoherent optical processing and passive synthetic aperture imaging are described more comprehensively in the articles [7,8] attached as the Appendices.

2
BASIC PRINCIPLE

Astronomers have for some time made use of interferometric techniques for astronomical imaging, from Michelson's simple two-aperture interferometer to sophisticated very long baseline interferometers that span the globe. They are all based on the van Cittert-Zernike theorem which relates the intensity distribution and the mutual coherence function of the fields in two widely separated planes.

Consider the system geometry is illustrated in Figure 1. An object field radiates according to its blackbody temperature and the emitted radiaiton is received at (x_1,y_1) and (x_2,y_2). Assuming that the emitted radiation is quasimonochromatic (or made so by spectral filtering), then by using the Huygen-Fresnel principle, the wave disturbances at (α_1,β_1) and (α_2,β_2) due to the radiation from the object field A can be written as [6].

$$E(x_1,y_1) = \frac{1}{\lambda}\iint_{\Sigma} E_o(\alpha_1,\beta_1)\frac{e^{-i(kR_1-\omega t)}}{R_1}\,d\alpha_1 d\beta_1 \qquad (1)$$

and

$$E(x_2,y_2) = \frac{1}{\lambda}\iint_{\Sigma} E_o(\alpha_2,\beta_2)\frac{e^{-i(kR_2-\omega t)}}{R_2}\,d\alpha_2 d\beta_2 \qquad (2)$$

where λ is the wavelength corresponding to the center frequency of the filter, $E_o(\alpha_1,\beta_1)$ and $E_o(\alpha_2,\beta_2)$ are the wave disturbances at (α_1,β_1) and (α_2,β_2), R_1 and R_2 are the distances between (α_1,β_1) - (x_1, y_1) and (α_2,β_2) - (x_2,y_2) respectively, k is the wave number and ω the angular frequency of the radiation. Since the radiation is assumed to be quasimonochromatic, we shall from here on, neglect the time varying

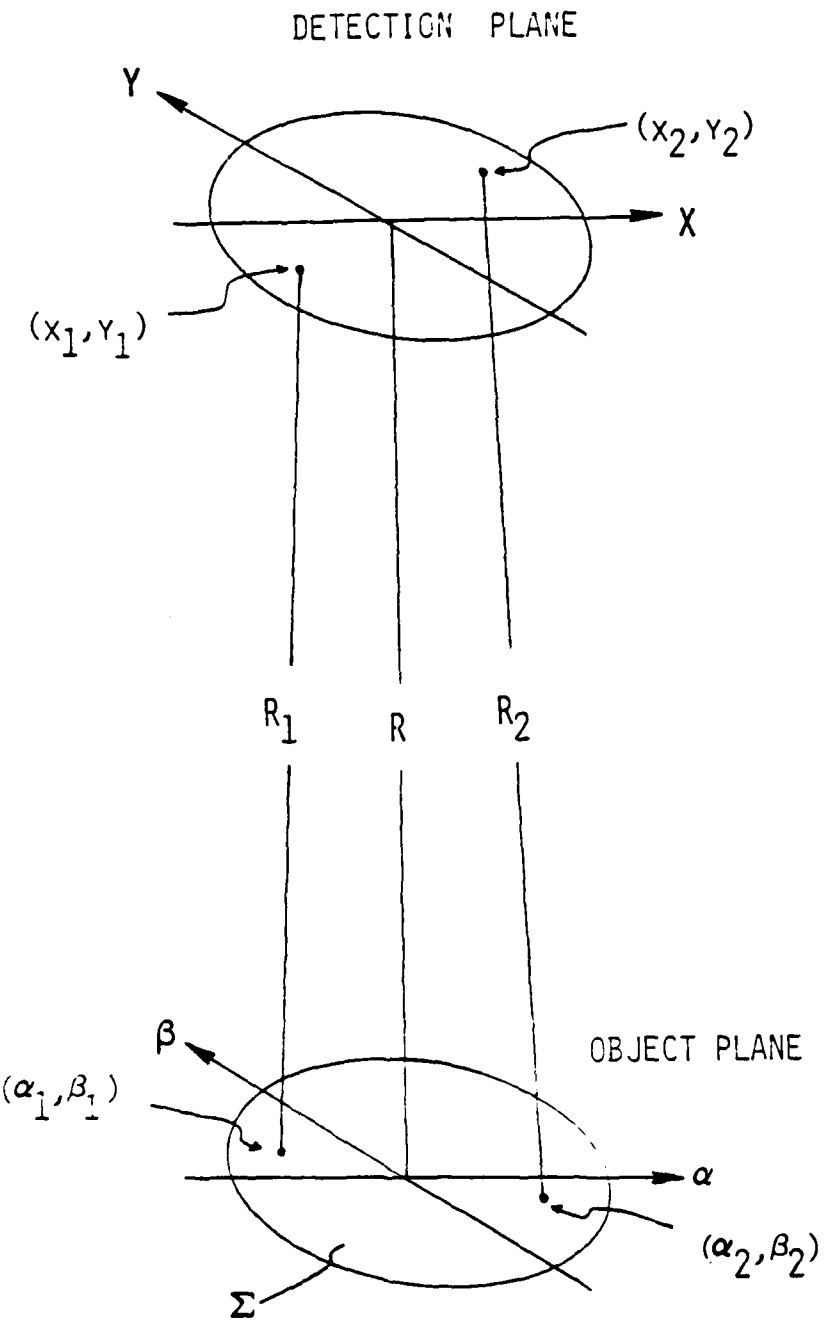

Figure 1: System Geometry for Passive Interferometric Imaging.

phase factor an let $E = E_0 e^{i\omega t}$.

The mutual intensity between Q and Q_2 is given by

$$J(x_1,y_1;x_2,y_2) = \langle E(x_1,y_1)E^*(x_2,y_2)\rangle \tag{3}$$

where $\langle\cdot\rangle$ denotes ensemble averaging. Substituting Eq. (1) and Eq. (2) into Eq. (3), we obtain

$$J(x_1,y_1;x_2,y_2) = \frac{1}{\lambda^2}\iint_{\Sigma}\langle E(\alpha_1,\beta_1)E^*(\alpha_2,\beta_2)\rangle \frac{e^{-ik(R_1-R_2)}}{R_1 R_2}\, dx_1 dy_1 dx_2 dy_2 \tag{4}$$

Since the emitted field is spatially incoherent,

$$\begin{aligned}\langle E(\alpha_1,\beta_1)\, E^*(\alpha_2,\beta_2)\rangle &= 0 \qquad \text{for } (x_1,y_1)=(x_2,y_2)\\ &= I(\alpha,\beta) \qquad \text{for } (\alpha_1,\beta_1)=(\alpha_2,\beta_2)=(\alpha,\beta)\end{aligned} \tag{5}$$

where $I(\alpha,\beta)$ is the intensity distribution at the object plane. The mutual intensity can therefore be simplified to

$$J(x_1,y_1;x_2,y_2) = \frac{1}{\lambda^2}\iint_{\Sigma} I(\alpha,\beta)\frac{e^{-ik(R_1-R_2)}}{R_1 R_2}\, d\alpha d\beta \tag{6}$$

The complex degree of spatial coherence (CDSC) is related to the mutual intensity by [6]

$$\mu(x_1,y_1;x_2,y_2) = \frac{J(x_1,y_1;x_2,y_2)}{\sqrt{I(x_1,y_1)\ I(x_2,y_2)}} \tag{7}$$

where

$$I(x_1,y_1) \approx I(x_2,y_2) \approx \iint_{\Sigma} \frac{I(\alpha,\beta)}{R^2}\, d\alpha d\beta \tag{8}$$

Let us assume that the α - β plane and the x-y plane are parallel to each other, we can then write

$$R_1^2 = (x_1 - \alpha)^2 + (y_1 - \beta)^2 + R^2 \tag{9}$$

where R is the separation between thetarget plane and the detection plane.

R_1 can be approximated by

$$R_1 = R + \frac{(x_1-\alpha)^2 + (y_1-\beta)^2}{2R} \tag{10}$$

and similarly

$$R_2 = R + \frac{(x_2-\alpha)^2 + (y_2-\beta)^2}{2R} \tag{11}$$

Thus,

$$R_1 - R_2 = \frac{(x_1^2 + y_1^2) - (x_2^2 + y_2^2)}{2R} - \frac{(x_1 - x_2)\alpha + (y_1 - y_2)\beta}{R} \tag{12}$$

Substituting Eq. 2-14 into Eq. 2-7 we obtain

$$\mu_{12}(u,v) = \frac{e^{i2\pi\Psi}}{\lambda^2} \iint_{\Sigma} I(\alpha,\beta) e^{i2\pi(u\alpha+v\beta)} d\alpha d\beta \Big/ \iint_{\Sigma} I(\alpha,\beta) d\alpha d\beta \tag{13}$$

where $u = (x_1 - x_2)/R\lambda$, $v = (y_1 - y_2)/R\lambda$ and

$$\Psi = \frac{(x_1^2+y_1^2)-(x_2^2+y_2^2)}{2R\lambda}$$

The CDSC, $\mu_{12}(u,v)$ is equal to the Fourier transform of the object intensity distribution multiplied by a quadratic phase. If the far field condition is satisfied, then $\psi \tilde{=} 0$ and $e^{i\psi} \tilde{=} 1$. The CDSC becomes

$$\mu_{12}(u,v) = K \iint_{\Sigma} I(\alpha,\beta) e^{i2\pi(u\alpha+v\beta)} d\alpha d\beta \tag{14}$$

where K is a complex constant.

We see that the CDSC is related to the intensity distribution of the object field by a Fourier transform relationship. We can therefore reconstruct the object image by measuring the two-dimensional coherence function and performing an inverse Fourier transform.

The CDSC can be obtained with Young's simple two-pinhole arrangement or equivalently, Michelson's stellar interferometer, by measuring the complex visiblity of the interference fringes. The complex fringe visiblity function is defined as

$$V(x_1,y_1;x_2,y_2) = \frac{2\sqrt{I(x_1,y_1)}\ \sqrt{I(x_2,y_2)}}{I(x_1,y_1) + I(x_2,y_2)}\ \mu(x_1,y_1;x_2,y_2) \tag{15}$$

Except for very near field conditions, we can as before make the approximation, $I(x_1,y_2) = I(x_2,y_2)$ and we have

$$V(u,v) \propto \mu(u,v) \tag{16}$$

To measure the CDSC via the visibility function is not very efficient since the interference pattern must be scanned out with a small detector to determine the phase and modulation depth of the sinusoidal fringe pattern. An alternate approach is to use a beam splitter to recombine the fields gathered at (x_1,y_1) and (x_2,y_2) such that they propagate coincidentally. The entire output can then be focussed on and detected by a photo detector. It can be shown that the output corresponds to the inphase portion of the Fourier transform sampled at spatial frequency (u,v) (see Appendix B). The quadrature part can be obtained by shifting the position of the beam splitter to generate a $\pi/2$ phase difference between the recombined fields. By changing the positions of (x_1,y_1) and (x_2,y_2), different spatial frequencies of the object is measured. A large aperture can then be synthesized in time.

We can see from Eq. 15 that the Fourier transform kernel is scaled by wavelength. This fact is used in synthetic aperture imaging systems to generate the radial fill of the synthetic aperture. This wavelength dependency however, also limits the instantaneous spectral bandwidth

that can be used with either the active or the passive systems. Opening the bandwidth too wide will produce a smearing effect in the phase history signal and reduce the system signal-to-noise ratio. This restriction does not pose any problem for active systems but it limits the performance of passive interferometric imaging systems. Natural emissions and illuminating sources are spectrally very wide band and the SNR of the images reconstructed with a passive interferometric imaging system is directly proportional to the instantaneous spectral bandwidth. System sensitivity can therefore be improved if a means can be found to increase the instantaneous spectral bandwidth without suffering the signal loss due to the wavelength dependency of Fourier transformation.

In the next section the use of an achromatic grating interferometer for passive synthetic aperture imaging of rotating objects in the visible region is described. The achromaticity of the grating interferometer permits the instantaneous spectral bandwidth to be widened up substantially while maintaining the capability to use wavelength diversity to achieve aperture fill. And as we shall show, the achromatic grating interferometer also offers other operational advantages over conventional interferometric systems when used for passive synthetic aperture imaging.

3
ACHROMATIC GRATING INTERFEROMETER

The achromatic grating interferometer has been studied extensively and applied to many applications [1,8-10]. Tai and Aleksoff in particular, has utilized it as an incoherent optical processor for real time Fourier transformation [10]. The transform operation is limited to a single dimension and it could create difficulties in some applications. This limitation however, does not represent any drawback for synthetic aperture imaging since under most operating conditions, a long baseline is available only along a single dimension (e.g., along the fuselage of an airplane).

Since the interferometer performs the correlation only along a single dimension at any one time, a two dimensional model, comprising of the direction of propagation and the direction of lateral separation of the fields to be correlated, will be used to describe the operation of the grating interferometer. In Figure 2, we show that geometry of a grating interferometer that can be used for passive synthetic aperture imaging. It is composed of three gratings of the same spatial frequency F. Light waves impinging on gratings G_1 and G_2 are diffracted and recombined at G_3 which is placed a distance d from the plane formed by G_1 and G_2. The gratings G_1 and G_2 also represents the input apertures and they have a width of A and are separated by a distance S. After being diffracted by G_3, the recombined fields propagate coincidentally and are focussed down onto a photo detector of width W_d. Let us assume as before that the object plane is sufficiently far away that the light emanated by a point source in the object scene may be considered to be a plane wave as it impinges on the input apertures of the grating interferometer. Thus, for a single point source of intensity $O(\alpha_o)$ located at a distance α_o from the optical axis as shown in Figure 3, the optical field just before it is diffracted by the grating G3 is equal to

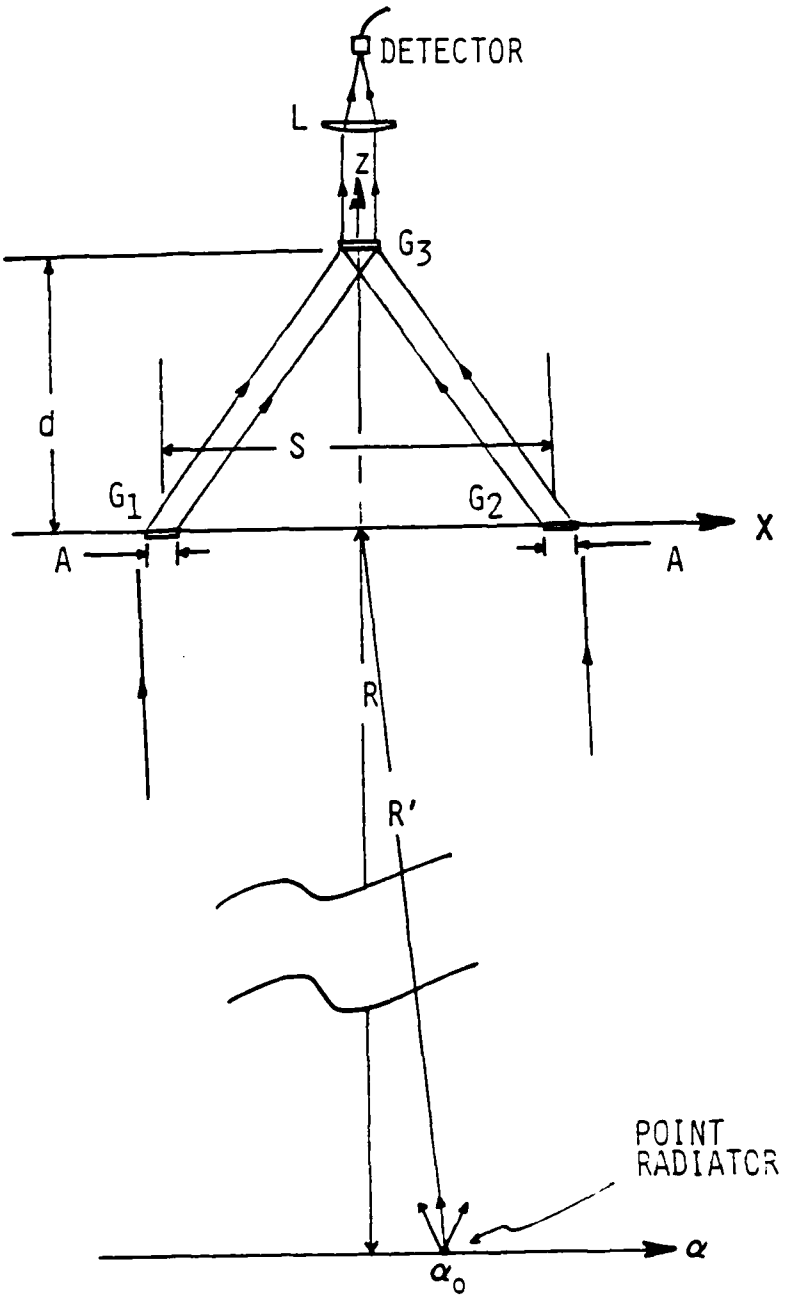

Figure 2: System Geometry for Passive Synthetic Aperture Imaging with a Grating Interferometer.

$$E(\alpha_o) = \sqrt{O(\alpha_o)} \left\{ \exp\left[i2\pi(p - F)x - ikR' \sqrt{1 - \lambda^2 p^2} - ikd \sqrt{1 - \lambda^2 (p - F^2)} \right] \right.$$

$$\left. + \exp\left[i2\pi(p + F)x - ikR' \sqrt{1 - \lambda^2 p^2} - ikd \sqrt{1 - \lambda^2 (p + F)^2} \right] \right\} \quad (17)$$

where F is the spatial frequency of the diffraction gratings, $p = \sin[\mathrm{atn}(\alpha_o/R)]/\lambda$ and $k=2\pi/\lambda$. The corresponding intensity distribution can be written as

$$I_G(\alpha) = CO(\alpha_o) \left\{ 1 + \cos\left[4\pi F x - \frac{2\pi d}{\lambda} \left(\sqrt{1 - \lambda^2 (p + F)^2} - \sqrt{1 - \lambda^2 (p - F)^2} \right) \right] \right\} \quad (18)$$

where C is an appropriate constant. Using a grating G3 with spatial frequency F to recombine the beams diffracted by G1 and G2, the field intensity is demodulated back to base band in terms of spatial frequency and the intensity distribution right after being diffracted by G3 becomes

$$I_o(\alpha_o) = CO(\alpha_o) \left\{ 1 - \cos\left[\frac{2\pi d}{\lambda} \left(\sqrt{1 - \lambda^2 (p + F)^2} - \sqrt{1 - \lambda^2 (p - F)^2} \right) \right] \right\} \quad (19)$$

If we expand the square-root terms into binomial series and keep only the first order terms, we obtain

$$I_G(\alpha_o) = CO(\alpha_o) \left[1 - \cos 2\pi \left(\frac{2F d \alpha_o}{R} \right) \right] \quad (20)$$

We see that the output intensity, to the first order, is not a function of wavelength. The object scene within the FOV of the interferometer can be considered as a superposition of incoherent point sources. The output intensity due to the entire scene can then be expressed as

$$I_o(u) \cong C \int_{\Sigma} O(\alpha)\, d\alpha + C \int_{\Sigma} O(\alpha) \cos(2\pi u\alpha)\, d\alpha$$

where

$$u = \frac{2Fd}{R} \tag{21}$$

which gives a cosine transform relationship together with a bias term. If we translate grating G3 laterally by 1/8 of a grating period, the phases of the two fields being recombined are shifted achromatically by $\pm\pi/4$. It can be shown that the output intensity becomes

$$I_o(u) \cong C \int_{\Sigma} O(\alpha)\, d\alpha + C \int_{\Sigma} O(\alpha) \sin(2\pi u\alpha)\, d\alpha \tag{22}$$

giving the sine transform of the intensity distribution of the incoherent source.

For a given value of F, d and R, the grating interferometer measures the source spectrum at a spatial frequency of u = Fd/R. Unlike the conventional system described earlier, the transform kernel is not wavelength dependent.

A more detailed discussion of the grating interferometer and its achromaticity are given in Appendices A and B.

4
PASSIVE SYNTHETIC APERTURE IMAGING

For a given interferometer geometry, the correlation output provides the value of the object spectrum at a single spatial frequency. The system geometry must be changed to generate transform data at other spatial frequencies in order to synthesize a two-dimensional aperture. First, if there is relative rotational motion about the optical axis between the object scene and the interferometer, transform data can be gathered along a circular arc in the transform plane. Second, if either the baseline or the detection wavelength is varied, transform data long a radial line in the transform plane is obtained. Combining these two effects, a two-dimensional aperture can be synthesized. The means to achieve such an aperture fill will be discussed below.

Let us assume for now that the interferometer is looking straight down at the object scene located at the optical axis. The interferometer output provides the transform data at a single point in the Fourier transform plane. As the object (or equivalently, the interferometer) rotates about the optical axis, data is gathered along a circular arc.

Radial fill of the synthetic aperture can be achieved with the use of baseline diversity or wavelength diversity. Since the spatial frequency measured is determined by $S/R\lambda$, it can be changed by varying S, the separation of the detection aperture (baseline) or λ, the detection wavelength. Baseline diversity can be accomplished with the grating interferometer by moving the three gratings closer or apart. However, it may not the desired mode of operation for synthetic aperture imaging since it requires the use of large input windows to accomodate the change in baseline. It is often more preferrable to keep the input aperture fixed and achieve the radial aperture via the use of wavelength diversity. On the surface, it may seem that the use of wavelength diversity with an achromatic system is contradictory. We note however, that the interferometer has a finite instantaneous bandwidth and the

whole band can be slided back and forth to obtain the wavelength diversity for radial aperture fill. This is accomplished by changing d, the separation between gratings G1-G2 and G3. Recall from Eq. 24 that the spatial frequency measured by the interferometer is equal to 2Fd/R. Changing d thus varies the spatial frequency measured. It can be seen from Figure 3 that changing d is also equivalent to changing the center wavelength of measurement λ.

The two means of aperture (circular and radial) fill can be used together to generate a two-dimensional aperture. Unlike tomographic imaging, synthetic aperture imaging systems generally gather transform data over an angular range much less than 90 degrees and the two-dimensional aperture synthesized is typically a segment of the an annulus as shown in Figure 4. The image (half-power) resolution in the ground plane is approximately equal to

$$\rho_\alpha \cong \frac{R\lambda}{A_u} = \frac{R\lambda^2}{S\Delta\lambda}$$

$$\rho_\beta \cong \frac{R\lambda}{A_v} = \frac{R\lambda}{2\,S\,\sin\left(\frac{\Delta\theta}{2}\right)} \qquad (23)$$

where $\Delta\theta$ is the angle of rotation. The resolution in the α direction is proportional to λ^2 instead of λ. It is because the size of the synthetic aperture is proportional to $\Delta\lambda/\lambda$, the aperture is larger for smaller λ if $\Delta\lambda$ is fixed. For example, a real aperture imaging system operating at 0.5 m with a 10 cm aperture can achieve a ground plane resolution of 5m x 5m at a range of 1000 km. A passive synthetic aperture imaging system with the same real aperture size and an aperture separation of 2m on the other hand, can achieve a ground plane resolution of 0.63m x 0.58m at the same distance with λ = 0.5 μm, $\Delta\lambda$ = 0.2 μm, and $\Delta\theta$ = 25°.

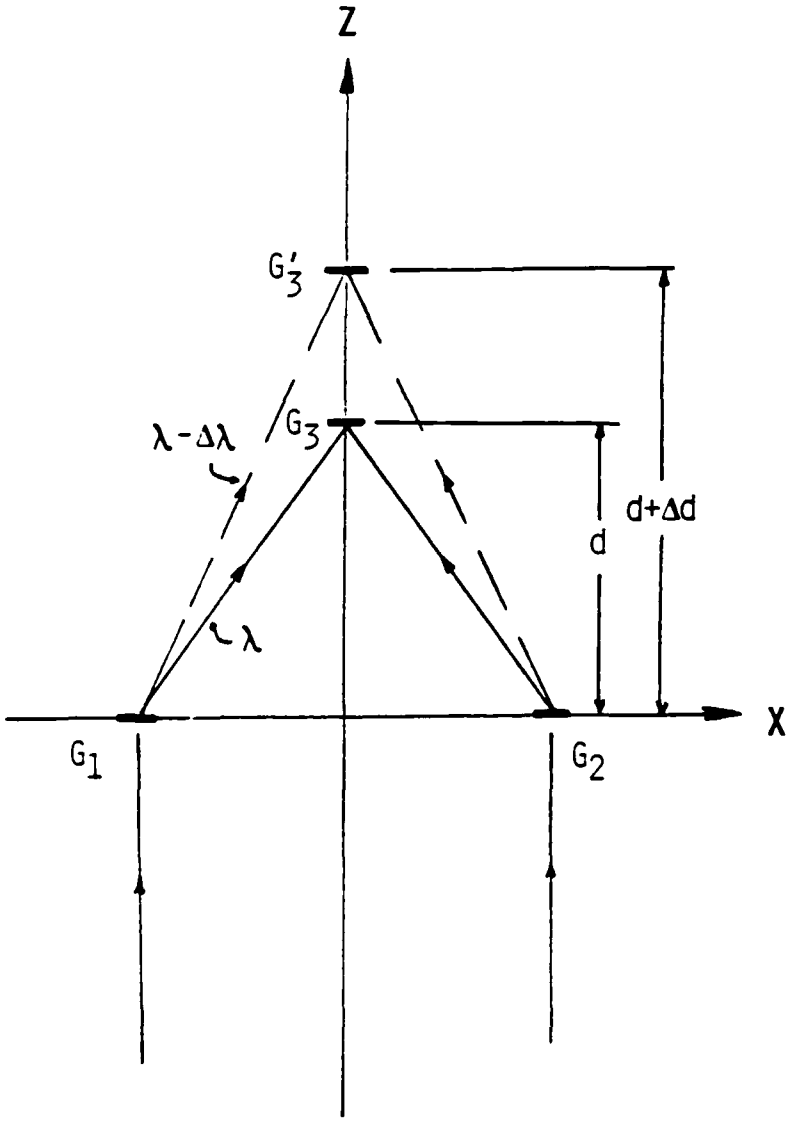

Figure 3: Wavelength Diversity as Implemented by the translation of Grating G_3.

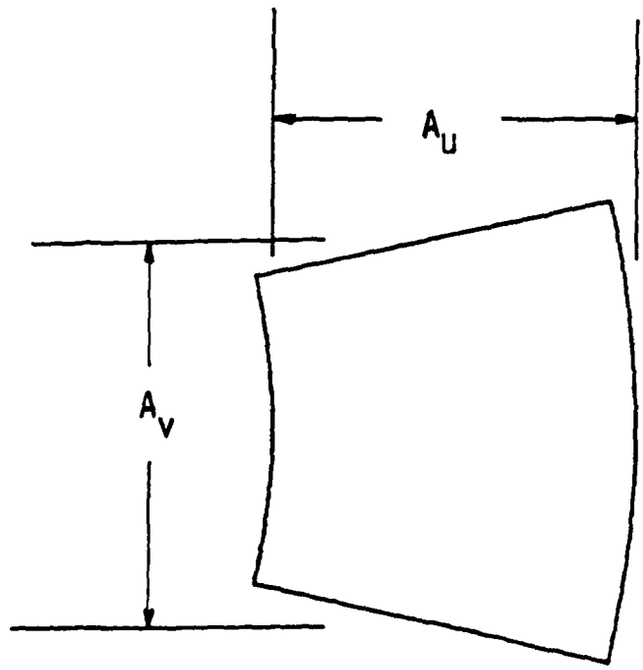

Figure 4 : Band Pass Synthetic Aperture Generated by Object Rotation and Wavelength Diversity.

We have shown (see Appendix B) that a substantially wider instantaneous spectral bandwidth can be used with the grating interferometer than with a conventional interferometer, thereby giving the grating interferometer better sensitivity. There are also operational advantages in using the grating interferometer. In a conventional system, the measurement wavelengths and thus the spatial frequencies, are selected with a bank of narrow band spectral filters. With the grating interferometer on the other hand, it is determined by the position of the grating G_3 which can be varied continuously. Therefore, continuous radial fill is difficult to achieve with conventional interferometers (without changing the baseline) but simple to implement with a grating interferometer. Due to the sampling requirements, measurement at many wavelengths is often required to generate an adequate aperture fill. The number of parallel chanels required could be fairly large (>30). The grating interferometer provides the option of using a single or a small number of parallel channels. The aperture fill is obtained by simply dithering a single or a small set of gratings.

The grating interferometer is also less sensitive to system vibration and accurate phase shifts can be more easily achieved. It is because the phases of a diffracted waves are determined mainly by the lateral position of the grating fringes. Moving a grating laterally by one grating period instead of one wavelength produces one full wave of phase shift. It is therefore many times less sensitive to component motion than conventional interferometers that employ mirrors and beam splitters.

A more comprehensive discussion of the use of the grating interferometer for passive synthetic aperture imaging is given in Appendix B.

5
MOVING TARGET SENSOR

In some applications, the ability of an interferometric sensor to measure a target spectrum at high spatial frequencies can be used without the need to build a full two-dimensional aperture. One such application is the detection of a moving unresolvable point target.

Moving target detection can be performed by various means such as the subtraction of time delayed images. These techniques however, is effective only if the target is of a resolvable size. The energy of an unresolved point object is spreaded over the resolution cell of the image and the resulting signal-to-noise ratio may not be adequate for unambiguous target detection. The SNR can be improved by high pass or bandpass filtering since the target-to-background energy ratio is larger at high spatial frequency than near dc for a point target. An interferometer with a long base line can be used to detect the presence of a moving point target that is too small to be resolved by the real imaging aperture. Once again, the need to operate with a narrow spectral bandwidth restricts the efficiency of conventional systems when used in a passive mode.

Consider the grating interferometer depicted earlier in Figure 2. The output intensity as a function of target position α_o was found to be approximately equal to

$$I_o(u) \simeq CO(\alpha_o)[1 + \cos(2\pi u\alpha_o)] \tag{24}$$

where C is the constant, $O(\alpha_o)$ is the intensity of the point object and $u = 2Fd/R$. for a point target moving linearly along the α direction, the output intensity becomes

$$I_o(u,t) \simeq CO(\alpha_o)\ [1 + \cos(2\pi u[\alpha_o + Tt])] \tag{25}$$

where T is the translation rate and we have assumed that the intensity of the point target does not change with position or time. A linearly moving target thus produces a sinusoidal output intensity which can be filtered to enhance the SNR. The achromaticity of the grating interferometer once again leads to better system sensitivity by allowing the use of a wider instantaneous spectral bandwidth.

6
SUMMARY

We have examined the uses of a grating interferometer for passive synthetic aperture imaging to achieve imaging resolution beyond that permitted by the collection aperture and as a moving target sensor to detect the presence of moving targets that are too small to be resolved. We have shown that the achromaticity of the grating interferometer allows the use of a wider instantaneous spectral bandwidth which in turn provides a better system sensitivity than conventional systems. In addition, the grating interferometer offers a simple means to achieve two-dimensional aperture fill and it is more tolerant to system vibration.

References

1) A. Tai, et.al., "Imaging Through Scattering Media by Interferometric Techniques," Appl. Opt. 20, p. 2484, 1981.

2) A. Tai and C. Aleksoff, "Imaging Through Scattering Media with Grating-Based Interferometer: Final Technical Report to U.S.A.R.O., ERIM 143900-8-F, Contract DAAG-79-C-0143, 1980.

3) J. Cederquist, et.al., "Partial Coherence Sensor Experiments," Final Technical Report to NOSC, ERIM 163400-36-F, Contract N66001-82-K-0251, 1984.

4) J. W. Goodman, "Statistical Properties of Laser Speckle Patterns," Laser Speckle and Related Phenomena, ed. J.C. Dainty, Chapter 2, Springer-Verlag, New York 1984.

5) R. A. Sprague, "Surface Roughness Measurement Using White Light Speckles," Applied Optics, Vol. 11, P. 2811, 1972.

6) M. Born and E. Wolf, Principles of Optics, (MacMillan Co. New York, 1964), Chapter 8.

7) A. Tai and C. Aleksoff, "Grating-Base Interferometric Processor for Real Time Optical Fourier Transformation," Applied Optics, Vol. 23, p. 2282, 1984.

8) A. Tai, "Passive Synthetic Aperture Imagery Using an Achromatic Grating Interferometer," Submitted to Applied Optics.

Appendix A

GRATING-BASED INTERFEROMETRIC PROCESSOR FOR REAL-TIME OPTICAL FOURIER TRANSFORMATION

Anthony M. Tai and Carl C. Aleksoff

Reprinted from Applied Optics, Vol. 23, page 2282, July 15, 1984

Grating-based interferometric processor for real-time optical Fourier transformation

Anthony M. Tai and Carl C. Aleksoff

A processing approach is introduced that is capable of performing 1-D real-time Fourier transformations on the intensity distribution of an incoherent optical input. The processing approach is based on grating interferometers, and the resulting processors are simple in structure and easily implemented. Possible processor configurations together with experimental results demonstrating the operation of the system are presented. Analyses are given comparing the grating interferometric processor to the Michelson stellar interferometer and the classical coherent optical processor.

I. Introduction

The Fourier transformation is a basic operation in many signal processing applications, and it has been implemented by various optical techniques. Coherent optical processors[1] can perform Fourier transformation in real time, but they have several familiar limitations. Most coherent optical processing schemes require the use of an incoherent-to-coherent converter which reduces the system speed, dynamic range, and linearity. An achromatic Fourier transform system[2,3] can be utilized to relax the temporal coherence requirement and improve the system SNR by reducing coherence noise. The spatial coherence requirement, however, is unchanged, and an incoherent-to-incoherent converter is still needed.

One-dimensional processing using bulk acoustical modulators or SAW devices,[4,5] on the other hand, are often too limited in their space–bandwidth product by physical constraints such as transducer frequency response, acoustical velocity, and acoustical attenuation. Moreover, processing with an acoustical modulator is limited to serial inputs. To be able to process parallel spatial inputs such as images, a spatial-to-temporal conversion is needed.

Incoherent optical processing techniques such as OTF synthesis[6,7] permit the use of incoherent optical inputs, but their applications are limited to a rather restrictive class of operation. For example, complex Fourier transformation has not been demonstrated. Cosinusoidal transformation was demonstrated by Mertz and Rogers[8] using a shadow casting technique. Such a technique operates in the geometric optics regime, and the achievable space–bandwidth is consequently small. The optical vector–matrix multiplier[9,10] can be configured to perform Fourier transformation; unlike other more conventional optical processors, the vector–matrix multiplier operates on discrete sampled signals. The difficulties in constructing and aligning a large 2-D mask and the limits on the densities of these masks restrict the space–bandwidth product that can be achieved in practice. The relative complexity of the system also diminished its attractiveness.

In this paper, we introduce an optical processor which belongs to a class of processor which we call interferometric processors. This processor operates on incoherent optical inputs, but its performance is closely related to coherent optical processing systems. An achromatic grating interferometer is used in our implementation of the processing approach. It is capable of producing and displaying in real time the real and imaginary parts of the Fourier transform of a 1-D incoherent optical input. Preliminary experimental results are presented to verify the theory and to demonstrate the processing approach.

II. Complex Degree of Spatial Coherence

Consider the system geometry illustrated in Fig. 1. The radiation emitted by a space-limited object field at the (α,β) plane is detected at far-field locations (x_1,y_1) and (x_2,y_2). If the radiation is quasi-monochromatic and spatially incoherent, it can be shown that the complex degree of spatial coherence (CDSC) is equal to[11]

The authors are with Environmental Research Institute of Michigan, Infrared & Optics Division, P.O. Box 8618, Ann Arbor, Michigan 48107.

Received 30 November 1983.
0003-6935/84/142282-10$02.00/0.

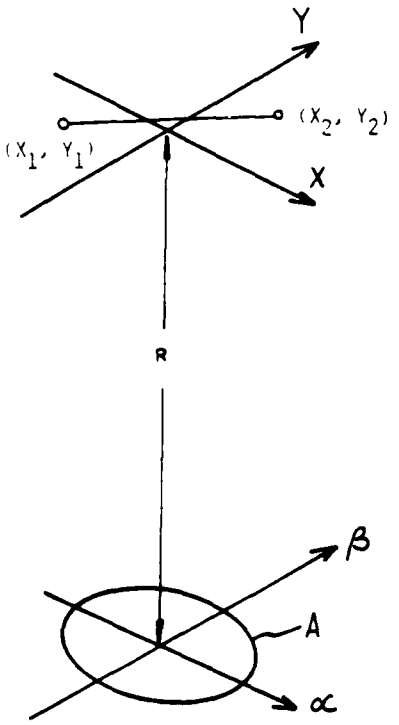

Fig. 1. System geometry relating the intensity distribution of an incoherent object field to the complex degree of spatial coherence at a detection plane in the far field.

$$C(u,v) = K \iint_A I(\alpha,\beta) \exp\left[\frac{-i2\pi}{\lambda}(u\alpha + v\beta)\right] d\alpha d\beta, \quad (1)$$

where

$$u = (x_1 - x_2)/R, \qquad v = (y_1 - y_2)/R,$$

and K is a constant.

We see that there is a Fourier transform relationship between the input intensity distribution and the CDSC at far field. This relationship is sometimes known as the van Cittert-Zernike theorem. Thus, to obtain the Fourier transform of the intensity distribution of an incoherent input, one merely has to devise a means to measure the CDSC at far field. This can be achieved interferometrically by measuring the complex visibility of the interference fringes formed between the fields at (x_1,y_1) and (x_2,y_2). The fringe visibility function is equal to

$$V[(x_1,y_1),(x_2,y_2)] = \frac{2\sqrt{I(x_1,y_1)}\sqrt{I(x_2,y_2)}}{I(x_1,y_1) + I(x_2,y_2)} \cdot C[(x_1,y_1),(x_2,y_2)]. \quad (2)$$

For a homogeneous incoherent input, $I(x_1,y_1) = I(x_2,y_2)$, and the CDSC is space invariant in the far field. Thus we may write

$$V(u,v) = C(u,v). \quad (3)$$

With the Michelson stellar interferometer and other similar interferometric imaging systems, the spatial frequencies are sampled by physically varying the separation of the detecting apertures. Such a sequential measurement scheme is too restrictive for use in a real-time processing system. The requirements that the input be quasi-monochromatic also makes the system very inefficient for inputs that are naturally polychromatic.

Roddier *et al.*[12] introduced a rotation shearing interferometer for astronomical imaging. Basically the input wave front is separated into two parts. One part is rotated 180° with a system of roof prisms or dove prisms and then recombined. At the center of the field which is the center of rotation there is no shear. Moving away from the center, increasing amounts of shear are introduced. Thus, unlike the Michelson stellar interferometer, all the spatial frequencies can be displayed at once. This technique is attractive for many applications, and it was suggested as an alternative to stellar speckle interferometry. However, similar to the Michelson stellar interferometer, it requires quasi-monochromaticity and is, therefore, rather inefficient in the processing of inputs that are spectrally wide band. George and Wang[13] combined the rotation shearing interferometer with an achromatic transform optical system and demonstrated polychromatic cosine transform. Their system, however, requires a system of prisms to perform the rotation and a multielement optical system for the achromatic transformation. Moreover, switching from cosine to sine transformation cannot be easily achieved due to the difficulty in realizing achromatic $\pi/2$ phase shifts using reflective and refractive optics.

In this paper, we introduce a grating-based achromatic optical processor. It is capable of producing, in real time, cosine and sine transformations of inputs that are spatially and temporally incoherent. One major advantage offered by grating-based systems is simplicity. The grating interferometric processor tends to require much less hardware than conventional systems making it easier to fabricate and set up. The simplicity of the grating system also makes the processor more compact and vibration resistant.

III. Achromatic Grating Interferometer

The achromatic grating interferometer has been studied extensively and applied to many applications. Chang and Leith[14-16] applied the interferometer to interferometric imaging and nondestructive testing. Leith and Roth[17,18] studied the noise performance of the interferometer and the synthesis of the convolution integral for linear filtering. Collins[19] demonstrated the construction of holograms and matched filters with incoherent light. Leith and Swanson[20] utilized the interferometer for the fabrication of noise-free diffractive optical elements. Tai and Aleksoff[21] employed the grating interferometer arrangement in an imaging system for improved imaging through scattering media.

Leith and Chang,[16] in particular, have recognized the ability of the grating interferometer to perform Fourier

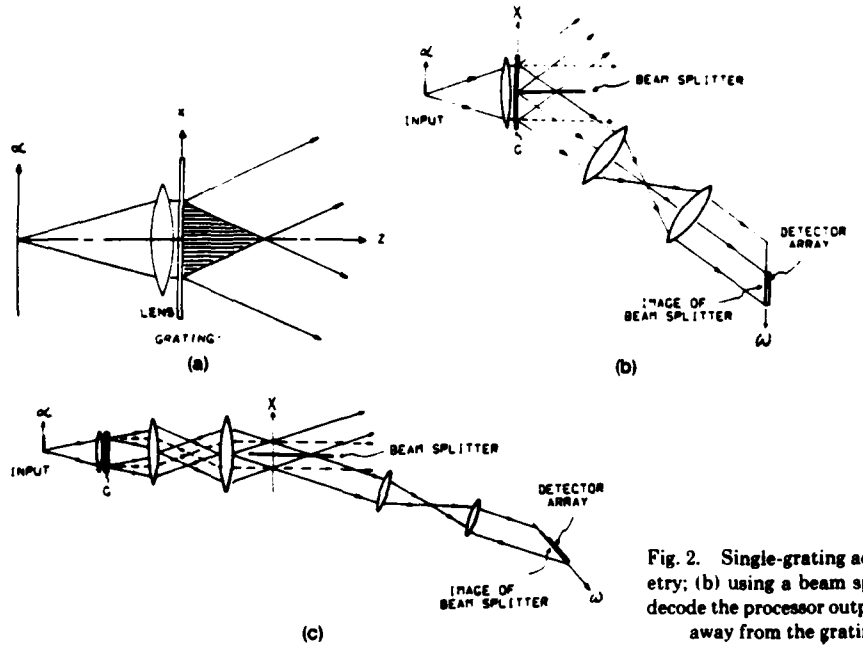

Fig. 2. Single-grating achromatic interferometer: (a) basic geometry; (b) using a beam splitter and a telescopic imaging system to decode the processor output; (c) imaging the fringe volume to a plane away from the grating to access the zero spatial frequency.

transformations. Their interest, however, was primarily in imaging where the image of an object was reconstructed by performing an optical transform with a coherent optical processor. To be able to utilize the interferometer as a processor, an appropriate decoding technique must be developed to produce a complex output that can be efficiently read out or interfaced to a computer.

The simplest achromatic grating interferometer that can be realized is composed of a single grating. Consider the optical arrangement depicted in Fig. 2(a). For a single point source located at $\alpha = \alpha_0$, the field amplitude in the volume where the ± 1 diffracted orders overlap is equal to

$$E(\alpha_0;x,z) = C\sqrt{S(\alpha_0)} \cdot |\exp[i2\pi(P_0 - F)x + ikz\sqrt{1 - \lambda^2(P_0 - F)^2}] + \exp[i2\pi(P_0 + F)x + ikz\sqrt{1 - \lambda^2(P_0 + F)^2}]|, \quad (4)$$

where $k = 2\pi/\lambda$, $S(\alpha_0)$ is the intensity of the point source, C is a constant, and $P_0 = \sin(\tan^{-1}\alpha_0/f)/\lambda$, f is the focal length of the lens, F is the spatial frequency of the grating, and λ is the wavelength of the source. The corresponding light intensity distribution in the fringe volume can be written as

$$I(\alpha_0;x,z) = |C|^2 S(\alpha_0)\left\{1 + \cos\left[4\pi Fx + \frac{2\pi z}{\lambda} \cdot [\sqrt{1 - \lambda^2(P_0 + F)^2} - \sqrt{1 - \lambda^2(P_0 - F)^2}]\right]\right\}. \quad (5)$$

Using a first-order approximation, the intensity distribution can be expressed as

$$I(\alpha_0;x,z) = |C|^2 S(\alpha_0)\left\{1 + \cos\left[4\pi F\left(x - \frac{z\alpha_0}{f}\right)\right]\right\}. \quad (6)$$

Now, if instead of having a single point source, we have a spatially incoherent line source with intensity distribution $f(\alpha)$ extending from $\alpha = 0$ to $\alpha = l$, the output intensity distribution within a constant factor is

$$I(x,z) = \int_0^l f(\alpha)\left[1 + \cos 4\pi F\left(x - \frac{z\alpha}{f}\right)\right] d\alpha. \quad (7)$$

The intensity along the optical axis at $x = 0$ is

$$I(z) = \int_0^l f(\alpha)(1 + \cos\omega\alpha)d\alpha = \int_0^l f(\alpha)d\alpha + \int_0^l f(\alpha)\cos\omega\alpha d\alpha, \quad (8)$$

where $\omega = 4\pi Fz/f$.

The first term is simply a constant bias, and the second term we recognize as the cosine transform integral. Thus by reading out the intensity distribution along the optical axis, we obtain the bipolar cosine transform of the 1-D input intensity distribution plus a constant bias. We emphasize that the expression in Eq. (8) is not a function of wavelength. The transformation is performed achromatically.

The single-grating interferometer provides an extremely simple means of achieving optical transformation achromatically. However, the information is displayed as an intensity distribution along the optical axis, which is rather inaccessible. In particular, the zero spatial frequency is located at $z = 0$, right at the surface of the grating. One way to read out the intensity distribution along the z axis is to place a very thin beam splitter along the z-y plane at $x = 0$ as shown in Fig. 2(b). The intensity distribution can then be imaged to a convenient output plane to be measured. Unfortunately, it is not straightforward to place such a beam splitter right up against the grating. It nevertheless can be done using special optics. One may image the fringe volume directly with a telescopic imaging system as

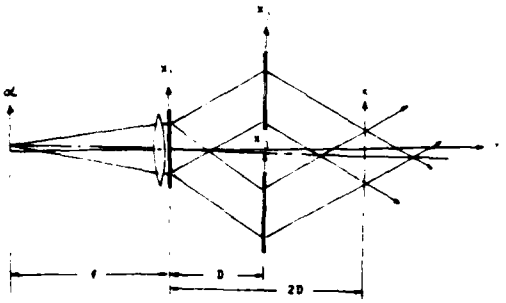

Fig. 3. Multiple-grating achromatic interferometer.

shown in Fig. 2(c) to make the fringe volume more accessible. However, the diffraction angles would be severely limited by the numerical apertures of the lenses. A better approach is to utilize a three-grating arrangement similar to that of Leith and Chang[14] as shown in Fig. 3. The first grating G_1 has a spatial frequency of F, the second and third gratings are coplanar, and both have a spatial frequency of $2F$. The input light field is split into two first orders and the first grating and then recombined by the second and third gratings, G_2 and G_3. A new fringe volume is formed about $z = 2D$, accessibly away from any grating. Moreover, spurious diffraction orders can now be easily removed to eliminate the spurious fringes and added bias that may otherwise be introduced. With a single point source located at $\alpha = \alpha_0$, the light field at the new fringe volume is equal to

$$\begin{aligned} E(\alpha_0;x,y) = C\sqrt{S(\alpha_0)}\cdot\{&\exp[i2\pi(P_0 - F)x \\ &+ ikD\sqrt{1-\lambda^2(P_0+F)^2} \\ &+ ik(z+D)\sqrt{1-\lambda^2(P_0-F)^2}] \\ &+ \exp[i2\pi(P_0+F)x + ikD\sqrt{1-\lambda^2(P_0-F)^2} \\ &+ ik(z+D)\sqrt{1-\lambda^2(P_0+F)^2}]\}. \end{aligned} \tag{9}$$

The corresponding light intensity distribution can be written as

$$\begin{aligned} I(x,z) = |C|^2 S(\alpha)\{&1 + \cos[4\pi Fx \\ &+ kz(\sqrt{1-\lambda^2(P_0+F)^2} - \sqrt{1-\lambda^2(P_0-F)^2})]\}, \end{aligned} \tag{10}$$

which can be approximated by

$$I(x,z) = |C|^2 S(\alpha)\left\{1 + \cos\left[4\pi F\left(x - \frac{z\alpha}{f}\right)\right]\right\}. \tag{11}$$

For a 1-D signal along the α axis ranging from 0 to l, the output intensity distribution becomes

$$I(x,z) = \int_0^l f(\alpha)\left\{1 + \cos\left[4\pi F\left(x - \frac{z\alpha}{f}\right)\right]\right\} d\alpha. \tag{12}$$

At $x = 0$, once again we have the cosine transform relationship

$$I(z) = \int_0^l f(\alpha)[1 + \cos(\omega\alpha z)]\, d\alpha. \tag{13}$$

To perform a Fourier transformation, both real and imaginary output data are required. By simply translating the grating G_2 along the X_2 direction by one-fourth of a period (i.e., $\pi/2$ phase shift), the light intensity distribution along the z axis becomes

$$I(z) = \int_0^l f(\alpha)[1 + \sin(\omega\alpha z)]\, d\alpha, \tag{14}$$

which is, of course, the sine transform of the input $f(\alpha)$. Thus both the real and imaginary parts of the complex transform output can be obtained. We may note that the shifting of the grating produces a $\pi/2$ phase shift for all wavelengths. The achromaticity of the system is maintained. This is in contrast to other interferometric systems using reflective or refracting optics.

Once again, the intensity distribution along the z axis can be read out by placing a thin beam splitter along the x-z plane as shown in Fig. 4. The intensity distribution along the beam splitter is mapped onto a convenient output plane outside the fringe volume using a one-to-one telescopic imaging system.

This simple implementation causes several problems. The beam splitter has to be very thin; a pellicle beam splitter might, therefore, be used. Pellicle beam splitters unfortunately have a tendency to vibrate. Although this is not a fundamental problem and can be solved using special optics, we decided to use an alternate arrangement for the demonstration.

The light distribution in the output fringe volume is equal to

$$I(x,y,z) = \int_0^l f(\alpha)\left\{1 + \cos\left[4\pi F\left(x - \frac{z\alpha}{f}\right)\right]\right\} d\alpha.$$

If we place a fourth grating with spatial frequency F at $z = z_0$ as shown in Fig. 5, the grating will demodulate the light back to zero spatial frequency, and the output light intensity becomes

$$I(z_0) = \int_0^l f(\alpha)\left[1 + \cos\left(\frac{4\pi F z_0 \alpha}{f}\right)\right] d\alpha, \tag{15}$$

which in effect gives the cosine transform of $f(\alpha)$ sampled at spatial frequency $4\pi F z_0/f$. By translating the

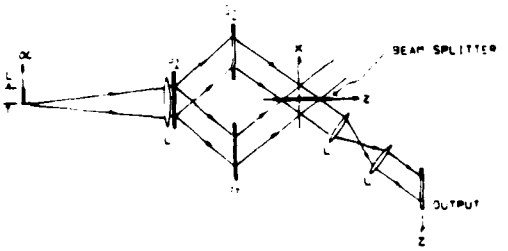

Fig. 4. Mapping the transform output in the fringe volume to a convenient output plane using a beam splitter.

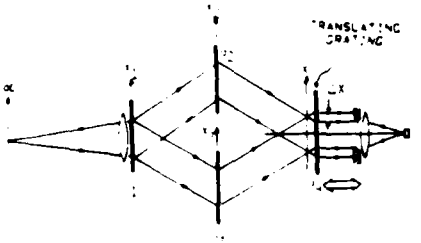

Fig. 5. Sampling of spatial frequencies with a translating fourth grating.

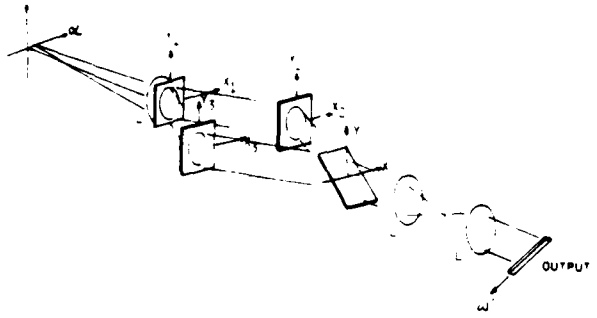

Fig. 6. Decoding the transform output with a tilted fourth grating.

fourth grating along the z axis over the entire fringe box, the cosine transform output can be scanned out. However, such a translation technique takes time, and our goal is real-time operation.

We note that Eq. (15) is not a function of x and y. The sampled cosine output can be obtained by measuring the intensity at any point of the output plane. If we tilt the fourth grating toward the x-z plane so that it traverses the fringe volume as illustrated in Fig. 6, different parts of the grating along the y direction will be sampling the intensity at different positions along the z direction. The output intensity distribution becomes

$$I(y) = \int_0^l f(\alpha)\left[1 + \cos\left(\frac{4\pi\alpha y F \tan\phi}{f}\right)\right] d\alpha, \tag{16}$$

which can be written as

$$I(\omega') = \int_0^l f(\alpha)d\alpha + \int_0^l f(\alpha)\cos(\omega'\alpha)d\alpha, \tag{17}$$

where

$$\omega' = (4\pi F y \tan\phi)/f,$$

and ϕ is the tilt angle of the fourth grating.

Once again, a biased output of the cosine transform is obtained. However, the spectrum is now displayed along the ω' direction, which is orthogonal to the α axis. The cosine spectrum, therefore, lies along a direction that is perpendicular to the 1-D input.

If we translate the fourth grating by one-eighth of a period (i.e., $\pm\pi/4$ phase shift), we obtain

$$I(\omega') = \int_0^l f(\alpha)d\alpha + \int_0^l f(\alpha)\sin(\omega'\alpha)d\alpha \tag{18}$$

or the sine transformation of $f(\alpha)$.

To perform complex Fourier transformations, we need both the real and imaginary parts. The cosine and sine transforms can be displayed simultaneously by using a split grating as the fourth grating at the output as shown in Fig. 7. The grating lines at the two halves of the grating are phase shifted by $\pi/4$. This produces a cosine transform at one side of the output and the sine transform at the other.

We note that the tilted grating decoding technique may also be applied to the single-grating interferometer by placing the tilted grating against the first grating transversing the fringe volume. However, the presence of spurious diffraction orders may substantially degrade the transform output. In addition, transform information near dc may not be displayed due to blockage by the edge of the tilted grating.

When only cosine transforms are performed, the input must be either single sided (i.e., $0 \le \alpha \le l$) or an even function [i.e., $f(\alpha) = f(-\alpha)$] to avoid ambiguity. With a dual-channel system, however, the input is no longer limited to being single sided or even. The processor is actually performing the decomposition

$$\int_{-\infty}^{\infty} f(\alpha)\exp(-i\omega\alpha)d\alpha = \underbrace{\int_{-\infty}^{\infty} f(\alpha)\cos(\omega\alpha)d\alpha}_{\mathcal{F}_R} \underbrace{-i\int_{-\infty}^{\infty} f(\alpha)\sin(\omega\alpha)d\alpha}_{\mathcal{F}_I}.$$

where $f(\alpha)$ is an arbitrary real and non-negative function, which in general is a combination of even and odd parts. That is, the decomposition is not in terms of the cosine transform of the even part and the sine transform of the odd part but rather in terms of $\mathcal{F}_r$ and $\mathcal{F}_I$, which are the real and imaginary parts, respectively, of the Fourier transform. In this operating mode, the input can extend from $-l$ to l with unique information on both sides, and the space–bandwidth product of the processor is in effect doubled. This doubling of the space–bandwidth product can be considered to occur because the system acts as a dual-channel processor simultaneously performing the real and imaginary parts of the Fourier transformation. A more detailed discussion on the space–bandwidth product of the grating interferometric processor is given in a later section.

IV. Experimental Results

An interferometric optical processor was set up using the configuration illustrated in Fig. 6. As the input, a ground glass diffuser was backilluminated by an unfiltered xenon arc lamp to produce an incoherent light source, which in turn was used to illuminate a slit and transparency. To test if the system can produce the correct Fourier transform output, a transparency with an intensity transmittance of $1 + \cos(2\pi g\alpha)$ was used. Thus the input is given by $f(\alpha) = \text{rect}[(\alpha - \alpha_0)L][1 + \cos(2\pi g\alpha)]$. The cosine/sine transform outputs were read out using a 1024-element linear detector array. In Fig. 8(a), we show the cosine transform output obtained with the interferometric processor. For comparison, we computed the Fourier transform of a function:

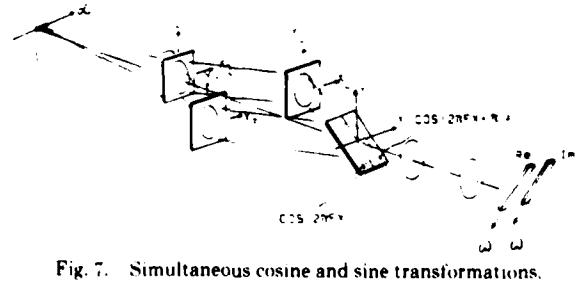

Fig. 7. Simultaneous cosine and sine transformations.

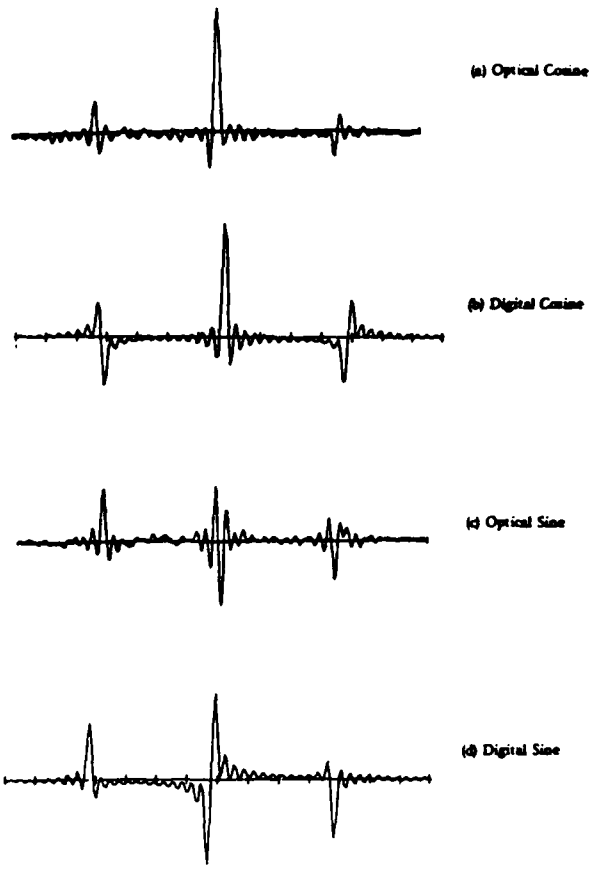

Fig. 8. Optically generated cosine and sine transforms vs the digitally computed versions.

$$f'(\alpha) = W(\alpha)\,\mathrm{rect}\left(\frac{\alpha-\alpha_0}{L}\right)[1+\cos(2\pi g\alpha+\phi)]\exp(i\theta), \quad (19)$$

where $\mathrm{rect}[(\alpha-\alpha_0)/L] = 1$ for $\alpha_0 - L/2 \le \alpha \le \alpha_0 + L/2$, $W(\alpha)$ is an apodizing factor added to account for the nonuniform illumination of the input, α_0 is the offset of the input from the axis, g is the spatial frequency, ϕ is the phase of the input cosine function, and θ is an arbitrary phase.

The choice of the grating position that is designated as cosine or sine transform is arbitrary and unimportant as long as an exact $\pi/2$ phase shift is introduced between the sine and cosine transforms and a consistency is maintained. The difference in the outputs caused by different initial choices of the grating position is simply a constant phase. (A similar situation arises in coherent optical processing where a coherent reference beam is introduced to measure the complex output of the optical processor.) In our experiment, the constant phase term $\exp(i\theta)$ was obtained by varying θ in the computation until the real part of the zero order of the digital Fourier transform matched that of the optical output. In Fig. 8(b), we show the computed real part of the Fourier transform. Except for a small phase difference, there is a very good correspondence between the optically obtained and digitally computed results. The small phase error might have been caused by irregularity in the local frequency of the gratings.

The fourth grating was then translated by one-eighth of a period to produce a $\pi/4$ phase shift on the recombined beams. The optically obtained sine transform output is shown in Fig. 8(c). For comparison, the corresponding computed imaginary part of the Fourier transform is shown in Fig. 8(d). Once again, the optical output matches the digitally computed result.

V. Comparison to a Michelson Stellar Interferometer

The operation of this system can be explained more intuitively by going back to the Michelson stellar interferometer. The Michelson stellar interferometer in its basic form is simply two apertures separated by a distance d as shown in Fig. 9(a). The CDSC is obtained by measuring the complex visibility of the fringes formed for different separations of the apertures. We see from Fig. 9(b) that we have a similar situation with the grating interferometer. The interfering light fields are sheared by an amount $\Delta x = z' \tan[\sin^{-1}(\lambda F)]$, where F is the spatial frequency of the grating. Thus, similar to the Michelson stellar interferometer, two parts of a wave front separated by a transverse distance Δx are made to interfere, and the resulting fringe visibility along the z axis, therefore, follows a Fourier transform relationship with the source intensity distribution. Unlike the Michelson interferometer where the visibility for each value of Δx must be measured separately, the grating interferometer presents the interference fringes for the different shear distances simultaneously at different positions of z. This interferometric optical

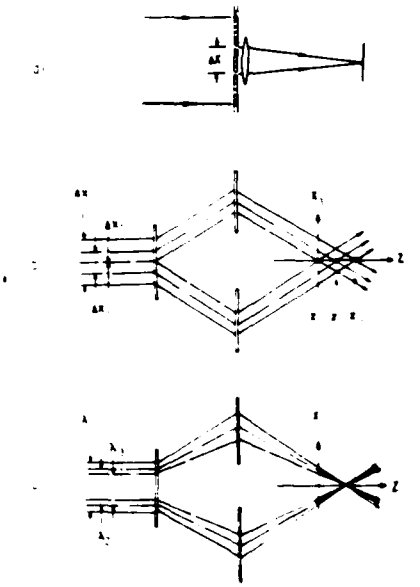

Fig. 9. Comparison with a Michelson-Stellar interferometer: (a) Michelson stellar interferometer; (b) simultaneous display of all spatial frequencies with the grating interferometer; (c) wavelength-dependent shearing of input wave front.

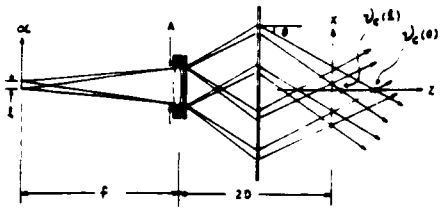

Fig. 10. Shifting of fringe volume for off-axis input point.

processor is, therefore, basically an interferometer that is capable of measuring in parallel the 1-D CDSC of a field emanated from a homogeneous incoherent line source at far field as created by the collimating lens.

The spatial frequency as measured by a Michelson interferometer is given by $u = 2\pi\Delta x/\lambda f$, which is wavelength dependent. A Michelson interferometer can, therefore, operate only with quasi-monochromatic radiation. To make the system achromatic, a variable amount of shear must be introduced so that $\Delta x(\lambda)/\lambda =$ constant. The amount of shear introduced by the grating interferometer varies with wavelength, since to the first order, $\Delta x = 2F\lambda z$, as illustrated in Fig. 9(c). The spatial frequency is thus $u = 4\pi Fz/f$, which is wavelength independent and hence achromatic.

VI. Comparison to Coherent Optical Processing

Although the interferometric processor operates on incoherent inputs, its performance characteristics are very similar to a coherent optical processor. For a coherent system, the transform relationship can be written as

$$F(p) = \int_{-\infty}^{\infty} f(\alpha) \exp\left(\frac{i2\pi\alpha P}{\lambda f}\right) d\alpha, \tag{20}$$

and for the interferometric optical processor,

$$F_R(z) = \int_{-\infty}^{\infty} f(\alpha) \cos\left(\frac{4\pi Fz\alpha}{f}\right) d\alpha \tag{21}$$

and

$$F_I(z) = \int_{-\infty}^{\infty} f(\alpha) \sin\left(\frac{4\pi Fz\alpha}{f}\right) d\alpha. \tag{22}$$

The difference between the two processors is in the scaling factors $2\pi/\lambda f$ and $4\pi F/f$. The scaling factor for a coherent optical processor is inversely proportional to wavelength, while the scaling factor for the interferometric processor is independent of wavelength. Hence the interferometric processor is equivalent to an achromatic Fourier transform system.[2,3]

For systems that use AO modulators or discrete sources (e.g., the vector–matrix multiplier) as input devices, the space–bandwidth product is typically input device limited and can be easily defined. For a coherent optical processor and an interferometric optical processor, on the other hand, the space–bandwidth product is usually processor-limited and is dependent on many factors such as the exact optical configuration, the f/No. of the transform or collimating lens, the aperture of the lens, and the performance of the lens. In the following, we compute the space–bandwidth product (SBWP) of the single-grating and the multiple-grating interferometers. The approximations and assumptions used in the computation are listed:

(1) The angular bandwidth of the gratings in the processor are very wide (e.g., surface relief gratings).

(2) The spurious diffraction orders are not a problem, and no stops are used in the system. (This assumption is always valid for systems that utilize beam splitters to demodulate the output. It is also valid for the multiple-grating system using a tilted fourth grating for output demodulated if the gratings are properly fabricated. The effects of spurious diffraction orders will be discussed in a later section.)

(3) The gratings are of sufficient size that the entire field over the full angular bandwidth is diffracted by the gratings.

(4) The field distribution along the optical z axis is considered as the output plane. [In actual system operation, it is necessary to transfer this output plane to a more accessible plane using a beam splitter or a grating. This analysis is directly applicable to a system that utilizes a beam splitter to demodulate the output (Fig. 4). With the use of a tilted fourth grating, however, the performance characteristic may be degraded in the decoding process, and the system SBWP may be lower than computed.]

(5) First-order approximations are used to describe the operation of the interferometer.

For both the single- and multiple-grating interferometric systems, except for the change in coordinate position, we have

$$I(z) = \int_{-t}^{t} f(\alpha)d\alpha + \int_{-t}^{t} f(\alpha)\cos(\omega\alpha)d\alpha,$$

where $\omega = 4\pi Fz/f$.

Consider specifically the multiple-grating processor as illustrated in Fig. 10. The fringe box translates down or up depending on the position of the input point. For a point input at $\alpha = \alpha_0$, the fringe box extends along the z axis up to

$$z' = \left(\frac{A}{2} - \frac{2D\alpha_0}{f}\right) \Big/ T.$$

where

$$T = \tan\left(\sin^{-1}\left\{\lambda F - \sin\left[\tan^{-1}\left(\frac{\alpha_0}{f}\right)\right]\right\}\right) \tag{23}$$

corresponding to a cutoff spatial frequency of

$$\nu_c(\alpha_0) = \frac{2F}{fT}\left(\frac{A}{2} - \frac{2D\alpha_0}{f}\right). \tag{24}$$

For the on-axis point $\alpha_0 = 0$, the cutoff frequency is a maximum and is given by

$$\nu_c(0) = \frac{A\cos\theta}{\lambda f}, \tag{25}$$

where

$$\theta = \sin^{-1}(F\lambda) \tag{26}$$

is the diffraction angle shown in Fig. 10. Notice that the cutoff frequency is wavelength dependent. We also

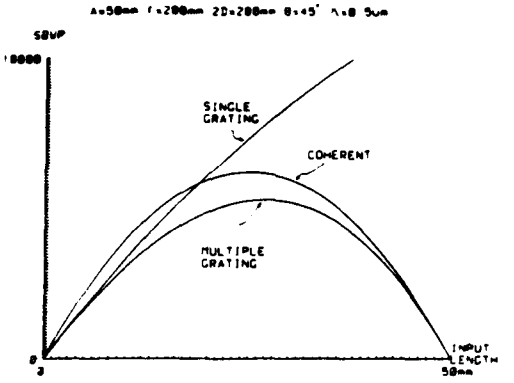

Fig. 11. Space-bandwidth products of a single-grating interferometric processor, a multiple-grating interferometric processor, and a coherent optical processor.

point out that, except for the cosine factor, Eq. (25) describes the highest frequency that can be coherently processed by a Fourier transform lens with aperture width A, focal length f, and the input placed a focal length in front of the lens. In fact, an expression equivalent to that of Eq. (24) for such a coherent processor is given in the Appendix.

Now consider an input signal of length $2l$, extending from $\alpha = -l$ to $\alpha = l$. The end point l establishes a cutoff frequency $\nu_c(l)$. Although one could define a space–bandwidth product (SBWP) given by the product of the line length by the maximum cutoff, i.e., $4l\nu_c(0)$, it is more meaningful for arbitrary inputs to establish the SBWP only as specified over the uniform (nontapering) part of the spectrum as given by the lowest cutoff frequency $\nu_c(l)$. Thus we define the SBWP as

$$\mathrm{SBWP}(l) = 4l\nu_c(l), \tag{27}$$

which with substitution from Eq. (24) becomes

$$\mathrm{SBWP}(l) = \frac{2l}{fT}\left(\frac{A}{2} - \frac{2Dl}{f}\right). \tag{28}$$

Equations (24)–(28) also hold for the single-grating interferometer by letting $D = 0$. The single-grating interferometer can be considered to be the limit of the multiple-grating interferometer as D approaches zero. It is seen from Eq. (28) that the SBWP is maximized for $D = 0$, i.e., for the single-grating interferometer.

It is worthwhile to compare the above results with those for a classical Fourier transform lens used as a coherent optical processor (see Appendix). The SBWP, defined in a similar way as for Eq. (28), for the coherent processor is

$$\mathrm{coh}[\mathrm{SBWP}(2l)] = 2l/\lambda \cdot (\sin|\tan^{-1}[(A - 2l)/f]|), \tag{29}$$

where the input extends from $-A/2$ to $2l - A/2$.

In Fig. 11, the SBWP is plotted as a function of the length of the input for the coherent optical processor and for the two-grating interferometer geometries. Note that for the multiple-grating interferometer and the coherent optical processor, there is an optimum input length. To maximize further the SBWP of the multiple-grating interferometer, it is necessary to minimize the length of the interferometer $2D$. (This is equivalent to moving the input closer to the Fourier transform lens in the case of a coherent optical processor.) As we shorten the interferometer, the gratings eventually collapse onto a single plane, and we essentially have the single-grating interferometer. (This is similar to putting the input right in front of the transform lens of the coherent optical processor.)

The above space–bandwidth product is computed from geometric considerations. A second factor that can limit the space–bandwidth product of the system is the dynamic range of the output detector array. The bias level is determined by the integrated input signal level

$$B = \int_{-l}^{l} f(\alpha)d\alpha.$$

As l increases so does the bias level. Thus the number of input points that can be processed for the worst case is equal to the dynamic range of the output detector. The space–bandwidth product, however, can be much larger if the transform of the input consists of only a small number of points (e.g., a sinusoidal input). In that case, the space–bandwidth product of the system is limited by the system geometry.

We should note that the same dynamic range limitation also applies to a coherent optical processor if the complex output is to be read out with a detector array. However, there is more flexibility with the coherent system. For example, if the input data are on a carrier and the information around dc is unimportant, the reference beam can be lowered to a level corresponding to the highest signal level in the desired portion of the output spectrum. With the interferometric processor, on the other hand, the bias is fixed at a level corresponding to the dc output.

We emphasize that unlike many other optical systems that utilize gratings (e.g., the achromatic Fourier transform system), spurious diffraction orders do not necessarily pose a problem for the grating interferometric processor. With the use of a beam splitter to decode the output, the spurious orders have minimal effect, since they propagate in directions away from the output plane as long as the angular subtend of the input is less than the diffraction angle of the grating. This is true for both the single-grating and multiple-grating arrangements utilizing beam splitters. For a multiple-grating system that employs a tilted grating to demodulate the output, the spurious diffraction orders are also not a serious problem. First, the higher diffraction orders propagate away from the output plane, and for the right arrangement they will not pose problem. The zero order does propagate toward the output plane, but it can be suppressed significantly. For example, if a thin sinusoidal phase grating is used, the powers in the various diffraction orders follow the Bessel functions. By adjusting the exposure in the fabrication of the grating to where the zeroth-order Bessel function goes to zero, the dc term can be substantially suppressed.

Furthermore, the zeroth order is incoherent with the first orders that are being combined (large path differences). Thus the effect of the dc term that remains is to add a small uniform bias to the output. Spurious orders, however, do create serious problems when using a tilted grating to decode the output of a single grating system, and such an arrangement is generally not desirable.

VII. Applications

The interferometric optical processor can be configured to perform operations currently accomplished by other optical processors. In addition, it can perform operations that cannot be easily done otherwise, since it operates on incoherent light.

For example, to process a temporal signal, the scanning electron beam of a CRT can be used to convert the temporal electrical signal into a spatial formatted light signal. The processed output is received by a detector array which is read out after integrating over the time of a complete scan of the electron beam. Such a system can operate over a large range of frequencies by varying the scan rate of the electron beam. The ease in obtaining the real and imaginary parts of the complex Fourier transform output gives the interferometric processor a potential advantage over optical systems using AO modulators and SAW devices.

The interferometer is a parallel processing device, and its capability is not fully utilized when used to process single-channel temporal signals. For applications where parallel inputs are available (e.g., from an antenna array), the inputs can be used to drive individual LEDs in a linear array. Together with an array of individually addressable detectors, the system can be used to perform n-point discrete Fourier transforms at a rate determined by the frequency response limit of the LEDs. As compared to the vector–matrix multiplier, the interferometric processor has the advantage of simplicity requiring only simple gratings and collimation optics instead of complicated 2-D masks and beam-forming optics.

More important, however, is the ability of the interferometric optical processor to operate on completely incoherent inputs. The system, therefore, has the potential to perform Fourier transformations on signals directly from the real world using light emanating from the object scene itself.

VIII. Summary

We have introduced an optical processor which is capable of performing complex spatial 1-D Fourier transforms on incoherent optical inputs. One possible implementation of the processing approach using a grating interferometer was presented, and the operation of an interferometric optical processor is experimentally demonstrated. The potential ability of the system to directly process images using the light emanated from an object scene removes limitations imposed by input devices and opens new avenues for optical processing. The research on this type of interferometric processor is still in it initial stages, and much has yet to be developed. The optical configurations presented are only examples of many other possible implementations of the interferometric optical processor. Alternative system configurations with different performance characteristics that are optimized for specific applications can be developed.

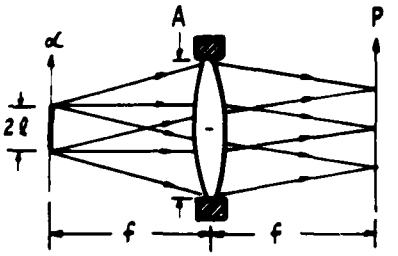

Fig. 12. Geometry of a coherent optical processor for the processing of real inputs.

The work was supported by the U.S. Army Research Office. Parts of this paper were presented at the International Optical Computing Conference, Apr. 1983.[22]

Appendix: Space–Bandwidth Product of a Coherent Optical Processor

For an optical Fourier transform lens to process the input signal without loss of information, all the light emanating from the input aperture must be passed by the lens aperture, i.e., no vignetting. Consider the 1-D optical processor illustrated in Fig. 12. At position α the cutoff frequency defined by geometry considerations is given by

$$\nu_c(\alpha) = \lambda^{-1} \sin|\tan^{-1}[(A - 2|\alpha|)/2f]|. \quad \text{(A1)}$$

Thus the cutoff frequency varies along the input aperture. It is possible to define a maximum space–bandwidth product via

$$\text{SBWP}_{\max} = 4l\nu_c(0), \quad \text{(A2)}$$

where the input is assumed to extend from $-l$ to $+l$ and the extra 2 comes from the two sidebands. However, to insure that the input is processed without loss of information, the highest spatial frequency of the input must be limited to $\nu_c(l)$. Then the SBWP becomes

$$\text{SBWP}(l) = 4l\nu_c(l). \quad \text{(A3)}$$

If the input is real, the transform is Hermitian. One sideband of the output spectrum can be discarded without loss of information. By placing the input asymmetrically from $-A/2$ to $2l - A/2$, the (one-sided) cutoff frequency becomes

$$\nu_c(2l) = \sin|\tan^{-1}[(A - 2l)/f]|, \quad \text{(A4)}$$

where $0 < l < A/2$. The SBWP becomes

$$\text{SBWP}'(l) = 2l\nu_c(2l). \quad \text{(A5)}$$

To determine the optimum input size for a given value of A and f, we let $2l = nA$ and take the partial derivative of Eq. (A3) to get

$$\frac{(2n-1)}{(1-n)^3} = \frac{A^2}{4f^2} \tag{A6}$$

and of Eq. (A5) to get

$$\frac{(2n-1)}{(1-n)^3} = \frac{A^2}{f^2}. \tag{A7}$$

For lenses with f/Nos. of $f/2$ or slower, n is nearly 0.5 for both cases. That is, the optimum SBWP tends to be obtained when the input aperture size is one-half of the lens aperture size.

References

1. J. W. Goodman, *Introduction to Fourier Optics* (McGraw-Hill, New York, 1968); F. T. S. Yu, *Introduction to Diffraction, Information Processing, and Holography* (MIT Press, Cambridge, 1973).
2. R. H. Katyl, "Compensating Optical Systems. 3: Achromatic Fourier Transformation," Appl. Opt. **11**, 1255 (1972).
3. G. M. Morris and N. George, "Frequency-Plane Filtering with an Achromatic Optical Transform," Opt. Lett. **5**, 446 (1980).
4. D. Das and F. M. M. Ayub, in *Applications of Optical Fourier Transforms*, H. Stark, Ed. (Academic, New York, 1982), Chap. 7.
5. N. J. Berg, J. N. Lee, M. W. Casseday, and B. J. Udelson, "Surface Wave Delay Line Acoustooptic Devices for Signal Processing," Appl. Opt. **18**, 2767 (1979).
6. A. W. Lohmann and W. T. Rhodes, "Two-Pupil Synthesis of Optical Transfer Functions," Appl. Opt. **17**, 1141 (1978).
7. W. Stoner, "Incoherent Optical Processing via Spatially Offset Pupil Masks," Appl. Opt. **17**, 2454 (1978).
8. G. L. Rogers, *Noncoherent Optical Processing* (Wiley, New York, 1968).
9. M. A. Monahan, K. Bromley, and R. P. Brocker, Proc. IEEE **65**, 121 (1977).
10. J. W. Goodman, A. R. Dias, and L. H. Woody, "Fully Parallel High-Speed Incoherent Optical Method for Performing Discrete Fourier Transforms," Opt. Lett. **2**, 1 (1978).
11. M. Born and E. Wolf, *Principles of Optics* (Pergamon, New York, 1975).
12. F. Roddier, C. Roddier, and J. Demarcq, J. Opt. (Paris) **9**, 145 (1978).
13. N. George and S. Wang, "Cosinusoidal Transforms in White Light," Appl. Opt. **23**, 787 (1984).
14. B. J. Chang, Ph.D. Thesis, U. Michigan, Ann Arbor (1974).
15. B. J. Chang and E. N. Leith, "Space-Invariant Multiple-Grating Interferometers in Holography," J. Opt. Soc. Am. **69**, 689 (1979).
16. E. N. Leith and B. J. Chang, "Image Formation with Achromatic Interferometer," Opt. Commun. **23**, 217 (1979).
17. E. N. Leith and J. A. Roth, "White Light Optical Processing and Holography," Appl. Opt. **16**, 2565 (1977).
18. E. N. Leith and J. A. Roth, "Noise Performance of an Achromatic Coherent Optical System," Appl. Opt. **18**, 2803 (1979).
19. G. D. Collins, "Achromatic Fourier Transform Holography," Appl. Opt. **20**, 3109 (1981).
20. E. N. Leith and G. J. Swanson, "Recording of Phase-Amplitude Images," Appl. Opt. **20**, 3081 (1981).
21. A. Tai, C. C. Aleksoff, and B. J. Chang, "Imaging Through Scattering Media by Interferometric Techniques," Appl. Opt. **20**, 2484 (1981).
22. A. Tai and C. C. Aleksoff, "An Incoherent Optical Processor for Real Time Complex Fourier Transformation," Proc. Soc. Photo-Opt. Instrum. Eng. **422**, 99 (1983).

Appendix B

PASSIVE SYNTHETIC APERTURE IMAGING USING AN ACHROMATIC GRATING INTERFEROMETER

Anthony M. Tai

ERIM

Passive Synthetic Aperture Imaging using an Achromatic Grating Interferometer

Anthony M. Tai

Infrared and Optics Division
Environmental Research Institute of Michigan
P.O. Box 8618
Ann Arbor, Michigan 48107

ABSTRACT

Synthetic aperture imaging with active systems is relatively well developed. The implementation of passive systems on the other hand, is being hindered by low SNR and the difficulty in achieving two-dimensional aperture fill. The achromaticity of the grating interferometer permits the use of a wider instantaneous spectral bandwidth to produce better SNR and it provides a simple means to synthesize a two-dimensional aperture. A passive synthetic aperture imaging approach implemented with an achromatic grating interferometer is described and laboratory experimental results are presented to demonstrate the proposed concept.

I. INTRODUCTION

Synthetic aperture imaging is a familiar development in the microwave wavelengths in the form of active SAR for fine image resolution imaging without resorting to the use of impossibly large antennae [1-3]. Relative motion between the sensor and the object scene is employed to generate synthetic aperture data. In particular, Walker showed [4] that through polar formatting, two-dimensional synthetic apertures of rotating objects can be generated with a range-Doppler imaging system. An imaging radar operating in such a mode is often referred to as a spot-light SAR since the radar is locked onto a fixed point in the target scene. Aleksoff [5] has also demonstrated the interferometric imaging of rotating objects in the visible wavelength using a fringe projection approach. Synthetic aperture systems utilizing either the range-Doppler or the fringe projection approaches are active systems. That is, radiations are launched by the imaging system and the fields reflected by the object scenes are measured. In this paper, a passive approach implemented with an achromatic grating interferometer for fine resolution imaging of incoherent scenes is described.

Passive synthetic aperture imaging techniques (or aperture synthesis) have been employed in astronomical imaging for sometime. The radio telescope is a prime example. An array of antennae are used with the earth rotation to generate the synthetic aperture [6]. While the operation of the active systems is based on coherent

diffraction theory, the operation of passive systems is based on the van Cittert-Zernike theorem. A coherent active system makes use of the Fourier transform relationship between the complex amplitudes at two widely separated (object and detection) planes. The synthetic aperture is generated by measuring the complex amplitude of the reflected radiation at the detection plane. The passive approach on the other hand, takes advantage of the Fourier transform relationship between the intensity distribution of an incoherent field at the object plane and the mutual coherence of the field at the detection plane. The synthetic aperture is therefore generated by measuring the spatial coherence of the field at the detection plane. The Fourier transform kernel is scaled by wavelength. This fact permits synthetic aperture imaging systems with fixed baselines to generate radial fills of the synthetic aperture. This wavelength dependency however, also limits the instantanteous spectral bandwidth that can be used with either the active or the passive systems. Too large an instataneous bandwidth can produce a smearing effect in the phase history signal (transform data) and reduce the system signal-to-noise ratio. This restriction does not pose any problem for active systems but it limits the performance of passive interferometric imaging systems. Natural emissions and illuminating sources are spectrally very wide band and the SNR of the images reconstructed with a passive interferometric imaging system is directly proportional to the instantaneous spectral bandwidth. System sensitivity can therefore

be improved if a means can be found to increase the instantaneous spectral bandwidth without suffering the signal loss due to the wavelength dependency of Fourier transformation.

In this paper, we introduce the use of an achromatic grating interferometer for passive synthetic aperture imaging of rotating objects in the visible region. The achromaticity of the grating interferometer permits the instantaneous spectral bandwidth to be widened substantially while maintaining the capability to use wavelength diversity to achieve aperture fill. And as we shall show, the achromatic grating interferometer also offers other operational advantages over conventional interferometric systems when used for passive synthetic aperture imaging. A system design approach and preliminary experimental results demonstrating the proposed passive synthetic aperture imaging concept are presented.

II. PASSIVE INTERFEROMETRIC IMAGING

Consider the system geometry as illustrated in Figure 1. An object field A radiates according to its blackbody temperature and the emitted radiation is received by an antenna pair located at Q_1 and Q_2. The emitted electromagnetic field is both temporally and spatially incoherent. However by filtering the received signals with a narrowband filter, the field may be treated as temporally coherent. (The filter bandwidth necessary to achieve coherency will be discussed later.) Let $E_o(\alpha_1, \beta_1)$ and $E_o(\alpha_2, \beta_2)$ be the wave disturbances on the object plane. By using the Huygens-Fresnel principle, the wave disturbances at (x_1, y_1) and (x_2, y_2) due to the radiation from the object scene can be written as [7]

$$E(x_1, y_1) = \frac{i}{\lambda} \iint_{\Sigma} E_o(\alpha_1, \beta_1) \frac{e^{-i(kR_1-\omega t)}}{R_1} d\alpha_1 \, d\beta_1 \qquad (1)$$

and

$$E(x_2, y_2) = \frac{i}{\lambda} \iint_{\Sigma} E_o(\alpha_2, \beta_2) \frac{e^{-i(kR_2-\omega t)}}{R_2} d\alpha_2 \, d\beta_2 \qquad (2)$$

where λ is the wavelength corresponding to the center frequency of the filter, R_1 and R_2 are the distance between (α_1, β_1) - (x_1, y_1) and (α_2, β_2) - (x_2, y_2) respectively, k is the wave number and ω the angular frequency of the radiation, and Σ represents the support of the object scene. Since the radiation is assumed to be quasimonochromatic, we shall from here on, neglect the time varying phase factor and let $E = E_o e^{i\omega t}$.

The mutual intensity between the fields at (x_1, y_1) and (x_2, y_2) is given by

$$J(x_1,y_1; x_2,y_2) = \langle E(x_1,y_1)E^*(x_2,y_2)\rangle \tag{3}$$

where $\langle\cdot\rangle$ denotes ensemble averaging. The complex degree of spatial coherence (CDSC) is related to the mutual intensity by

$$\mu(x_1,y_1, x_2,y_2) = \frac{J(x_1,y_1; x_2,y_2)}{\sqrt{I(x_1,y_1)I(x_2,y_2)}} \tag{4}$$

Using the Fresnel approximation, it can be shown that [6]

$$\mu_{12}(u,v) = \frac{\frac{e^{i2\pi\psi}}{\lambda^2} \iint_{\Sigma} I(\alpha, \beta)\, e^{i2\pi(u\alpha+v\beta)}\, d\alpha\, d\beta}{\iint_{\Sigma} I(\alpha, \beta)\, d\alpha\, d\beta} \tag{5}$$

where $u = (x_1 - x_2)/R\lambda$ and $v = (y_1 - y_2)/R\lambda$ and $\psi = [(x_1^2 + y_1^2) - (x_2^2 + y_2^2)]/2R\lambda$. The CDSC, $\mu_{12}(u, v)$, is equal to the Fourier transform of the object intensity distribution multiplied by a quadratic phase. If the far field condition is satisfied, then $\psi = 0$ and $e^{i2\pi\psi} \approx 1$, the CDSC becomes

$$\mu_{12}(u, v) = K \iint_{\Sigma} I(\alpha, \beta)\, e^{i2\pi(u\alpha+v\beta)}\, d\alpha\, d\beta \tag{6}$$

where K is a complex constant.

We see that the CDSC is related to the intensity distribution of the object field by a Fourier transform relationship. We can therefore reconstruct the object image by performing an inverse Fourier transform on the CDSC function.

III. CONVENTIONAL APPROACHES

The CDSC can be obtained with Young's simple two-pinhole arrangement or equivalently, Michelson's stellar interferometer, by measuring the complex visibility of the interference fringes. The complex fringe visibility function is defined as

$$V(x_1,y_1;\ x_2,y_2) = \frac{2\sqrt{I(x_1,y_1)}\quad\sqrt{I(x_2,y_2)}}{I(x_1,y_1) + I(x_2,y_2)}\ \mu(x_1,y_1;\ x_2,y_2) \quad (7)$$

Except for very near field conditions, we can generally make the approximation, $I(x_1,y_1)) = I(x_2,y_2)$ and we have

$$v(u,v) = \mu(u,v). \quad (8)$$

To measure the CDSC via the visibility function is not very efficient since the interference pattern must be scanned out with a small detector to determine the phase and modulation depth of the sinusoidal fringe pattern. An alternate approach is to use a beam splitter to recombine the fields gathered at (x_1,y_1) and (x_2,y_2) such that they propagate coincidentally. The entire output can then be focussed on and detected by a photo detector. The output, as we shall show, corresponds to the inphase portion of the Fourier transform sampled at spatial frequency (u, v). The quadrature part can be obtained by shifting the position of the beam splitter to generate a $\pi/2$ phase difference between the recombined fields. By changing the positions of (x_1,y_1) and (x_2,y_2), different spatial frequencies of the object is measured. A large aperture can then be synthesized in time.

In interferometric imaging as described above, the detected field is assumed to be quasimonchromatic. Natural emission and illuminating sources tend to be spectrally very wide band. To obtain coherency, the instantaneous spectral bandwidth of the received signal must be limited with a narrow band spectral filter. In the following, we examine the maximum instantaneous spectral bandwidth that can be used with a conventional system. A two-dimensional analysis will be used for two reasons. First, the number of terms is reduced, making the analysis easier to understand. Second, the interferometer itself is a one-dimensional system, performing at any single moment, the correlation of the fields between two points in the detection plane. A two-dimensional model comprised of the direction of propagation and the direction of the lateral separation (or shears) of the fields to be correlated, thus provides an adequate description of the system operation at any one time.

Consider a single point radiator in the far field as illustrated in Figure 2. The source is assumed to be located so far away that the field detected by the two detection apertures can be considered to be parts of a plane wave with the angle of incidence determined by the position of the source. The fields at the two apertures can be described by

$$E_1(\alpha_0) = \sqrt{o(\alpha_0)}\, e^{-i\frac{2\pi}{\lambda}\left[(R'+\Delta r)\sqrt{1-\lambda^2 p^2}\right]}$$

and

$$E_2(\alpha_o) = \sqrt{o(\alpha_o)}\, e^{-i\frac{2\pi}{\lambda}\left[(R'-\Delta r)\sqrt{1-\lambda^2 p^2}\right]} \tag{9}$$

where R' is the target range. $o(\alpha_o)$ is the field intensity at the detection plane due to a point source located at a distance α_o from the optical axis, and $p = \sin(\text{atn}\,[(\alpha_o/R)]/\lambda) \approx \alpha_o/R\lambda$ is the spatial frequency of the incident plane wave. (For a 2-dimensional object field, α_o is the position of the point source after it is projected onto the α axis.)

The total path difference from the source to the two detection apertures is

$$2\Delta r \approx \frac{S\alpha_o}{R}$$

where S is the separation of the apertures. If the fields are made to interfere with each other, the correlation output is equal to

$$I(\alpha_o) = C\, o(\alpha_o)\left[1 - \cos\left(\frac{4\pi\Delta r}{\lambda}\sqrt{1-\lambda^2 p^2}\right)\right] \tag{10}$$

where C is a complex constant. Using the Fresnel approximation, we have

$$I(\alpha_o) = C\, o(\alpha_o)\left\{1 - \cos\left[\frac{4\pi\Delta r}{\lambda}\left(1 - \frac{\lambda^2 p^2}{2}\right)\right]\right\}$$

$$= C\, o(\alpha_o)\left\{1 - \cos\left[\frac{2\pi\alpha_o S}{\lambda R}\left(1 - \frac{\alpha_o^2}{2R^2}\right)\right]\right\} \tag{11}$$

For small α_o,

$$\frac{\alpha_o^2}{2R^2} << 1,$$

we can further approximate the correlation output intensity and obtain

$$I(\alpha_o) = C\, o(\alpha_o) \left[1 + \cos\,(2\pi u \alpha_o)\right] \tag{12}$$

where

$$u = \frac{S}{\lambda R}\ .$$

Integrating over the entire object scene, we obtain a cosine transformation relationship plus a bias term.

$$I_o(u) = c \int_{\Sigma} o(\alpha_o)\, d\alpha_o + C \int_{\Sigma} o(\alpha_o) \cos\,(2\pi u \alpha_o)\, d\alpha_o \tag{13}$$

by adjusting the optics such that a $\pi/2$ phase difference is inserted between the two interfering fields, it can be shown that the correlation output intensity becomes

$$I_o(u) = C \int_{\Sigma} o(\alpha_o)\, d\alpha_o + C \int_{\Sigma} o(\alpha_o) \sin\,(2\pi u \alpha_o)\, d\alpha_o \tag{14}$$

Both the inphase and quadrature components of the Fourier transform can therefore be obtained.

The transform kernel $u = S/\lambda R$ is wavelength dependent. To see how wide an instantaneous spectral bandwidth can be used with a conventional interferometer, let us restrict the maximum phase misregistration to 1/4 of a wave. That is,

$$\frac{S\alpha_o}{\lambda R} - \frac{S\alpha_o}{(\lambda + \Delta\lambda)R} \leq \frac{1}{4}\ .$$

The instantaneous spectral bandwidth must then be limited to

$$\Delta\lambda \leq \frac{\lambda^2 R}{4(S\alpha_o - \frac{\lambda R}{4})} \tag{15}$$

for $\alpha_o = 0$ (i.e. an on-axis point source), we have $\Delta\lambda \leq \lambda$, the spectral bandwidth is unlimited. This is to be expected. For a point source at the optical axis, the path difference to the two detection apertures is zero.

The instantaneous spectral bandwidth decreases with increasing α_o. With the "spotlight" mode of synthetic aperture imaging, the system field of view (FOV) is defined by the footprint of the real aperture and it is locked on to a fixed point in the target scene. Thus, for a point target located at the edge of the FOV, we have $\alpha_o = R\lambda/A$ where A is the diameter of the detection aperture. The instantaneous spectral bandwidth that can be used with a conventional system for passive synthetic aperture imaging is therefore equal to

$$\Delta\lambda \leq \frac{\lambda^2 R}{4(\frac{SR\lambda}{A} - \frac{\lambda R}{4})} = \frac{\lambda A}{4S} . \tag{16}$$

For example, if $\lambda = 0.55$ μm, and $A/S = 1/20$, then $\Delta\lambda \leq 6.3$ nm.

IV. ACHROMATIC GRATING INTERFEROMETER

The achromatic grating interferometer has been studied extensively and applied to many applications [8-11]. Tai and Aleksoff in particular, has utilized it as an incoherent optical processor for real time Fourier transformation [11]. The transform operation is limited to a single dimension and it could create difficulties in some applications. This limitation however, does not represent any drawback for synthetic aperture imaging since under most operating conditions, a long baseline is available only along a single dimension (e.g., along the fuselage of an airplane).

For the same reasons stated earlier, a two-dimensional model will be used to describe the operation of the grating interferometer. In Figure 3, we show the basic geometry of a grating interfermeter that can be used for passive synthetic aperture imaging. It is composed of three gratings of the same spatial frequency F. Light waves impinging on gratings G_1 and G_2 are diffracted and recombined at G_3 which is placed a distance d from the plane formed by G_1 and G_2. The gratings G_1 and G_2 also represents the input apertures and they have a width of A and are separated by a distance S. After being diffracted by G_3, the recombined fields propagate coincidentally and are focussed down onto a photo detector of width W_d. Let us assume as before, that the object plane is sufficiently far away that the light field emanated by a point source in the object scene may be considered to be a plane wave as it impinges on the

input apertures of the grating interferometer. Thus, for a single point source of intensity $O(\alpha_o)$ located at a distance α_o from the optical axis as shown in Figure 3, the field right before it is diffracted by the grating G3 is equal to

$$E(\alpha_o) = \sqrt{O(\alpha_o)} \left\{ \exp\left[i2\pi(p - F)x - ikR' \sqrt{1 - \lambda^2 p^2} - ikd \sqrt{1 - \lambda^2 (p - F)^2} \right] + \exp\left[i2\pi(p + F)x - ikR' \sqrt{1 - \lambda^2 p^2} - ikd \sqrt{1 - \lambda^2 (p + F)^2} \right] \right\} \tag{17}$$

where F is the spatial frequency of the diffraction gratings, $p = \sin[\text{atn}(\alpha_o/R)]/\lambda$ and $k = 2\pi/\lambda$. The corresponding intensity distribution can be written as

$$I_G(\alpha) = CO(\alpha_o) \left\{ 1 + \cos\left[4\pi F x - \frac{2\pi d}{\lambda} \left(\sqrt{1 - \lambda^2 (p + F)^2} - \sqrt{1 - \lambda^2 (p - F)^2} \right) \right] \right\} \tag{18}$$

where C is an appropriate constant. Using a grating G3 with spatial frequency F to recombine the beams diffracted by G1 and G2, the field intensity is demodulated back to base band and the intensity distribution right after being diffracted by G3 becomes

$$I_o(\alpha_o) = CO(\alpha_o) \left\{ 1 - \cos\left[\frac{2\pi d}{\lambda} \left(\sqrt{1 - \lambda^2 (p + F)^2} - \sqrt{1 - \lambda^2 (p - F)^2} \right) \right] \right\} \tag{19}$$

If we expand the square-root terms into binomial series and keep only the first order terms, we obtain

$$I_G(\alpha_o) = CO(\alpha_o)\left[1 - \cos 2\pi\left(\frac{2Fd\alpha_o}{R}\right)\right] \qquad (20)$$

We see that the output intensity, to the first order, is not a function of wavelength. The object scene within the FOV of the interferometer can be considered as a superposition of incoherent point sources. The output intensity due to the entire scene can then be expressed as

$$I_o(u) \cong C\int_{\Sigma} O(\alpha)\, d\alpha + C\int_{\Sigma} O(\alpha)\cos(2\pi u\alpha)\, d\alpha \qquad (21)$$

where

$$u = \frac{2Fd}{R}$$

which gives a cosine transform relationship together with a bias term. If we translate grating G3 laterally by 1/8 of a grating period, the phases of the two fields being recombined are shifted achromatically by $\pm\pi/4$. It can be shown that the output intensity becomes

$$I_o(u) \cong C\int_{\Sigma} O(\alpha)\, d\alpha + C\int_{\Sigma} O(\alpha)\sin(2\pi u\alpha)\, d\alpha \qquad (22)$$

giving the sine transform of the intensity distribution of the incoherent source.

For a given value of F, d and R, the grating interferometer measures the source spectrum at a spatial frequency of $u = Fd/R$. Unlike the conventional system described earlier, the transform kernel is not wavelength dependent.

V. ACHROMATICITY

The achromaticity of the grating interferometer can be explained more intuitively by noting that the spatial frequency measured is equal to the $u(\lambda) = S/\lambda R$ where S is the lateral separation of the fields being correlated. To make the measurements achromatic, it is necessary that S be also wavelength dependent such that $u = S(\lambda)/\lambda R =$ constant. The grating interferometer satisfies this requirement to the first order by the fact that different wavelengths are diffracted at different angles such that at a given distance d where the fields from the two inputs apertures are recombined, the separation S of the fields being correlated are approximately proportioned to λ as illustrated in Figure 4. The range of lateral shear for given grating separation S is limited to $S \pm A/2$. If the interferometer is achromatic, then

$$\frac{R\lambda}{S(\lambda)} = \text{Constant.} \tag{23}$$

Thus,

$$\frac{R(\lambda + \Delta\lambda/2)}{S + A} = \frac{R(\lambda - \Delta\lambda/2)}{S - A} \tag{24}$$

and the instantaneous spectral bandwidth of an achromatic system is equal to

$$\Delta\lambda_1 = \frac{2A\lambda}{S} \tag{25}$$

The bandwidth is 8 times wider than that of a conventional system as computed earlier (see Eq. 16). The grating interferometer is

achromatic only to the first order. There is no guarentee yet that it is achromatic over the desired spectral bandwidth of $\Delta\lambda_1$.

In the following, the achromaticity of the grating interferometer is analyzed using a third order analysis.

In the previous section, we have shown that for a point source located a distance α from the axis, the output intensity can be approximated to the first order by

$$I_o(\alpha) = CO(\alpha)\left[1 - \cos\left(\frac{4\pi Fd\alpha}{R}\right)\right] \tag{26}$$

The grating interferometer is thus achromatic to the first order if the far field condition is met. If we expand Eq. 19 and keep all the terms up the third order however, we obtain

$$I_o(\alpha) \cong CO(\alpha)\left\{1 - \left[\cos 2\pi\lambda\rho Fd\left(2 + \lambda^2F^2 + \lambda^2\rho^2 + \frac{3}{8}F^4\lambda^4 + \frac{5}{4}\rho^2F^2\lambda^4\right)\right]\right\} \tag{27}$$

Since the FOV is confined to within the foot print of the real aperture, p generally is small and we can further approximate the output intensity distribution by

$$I_o(\alpha) = CO(\alpha)\left\{1 - \cos\left[\frac{2\pi Fd\alpha}{R}\left(2 + \lambda^2F^2 + \frac{3F^4\lambda^4}{8}\right)\right]\right\} \tag{28}$$

We find that the system is not achromatic to the third order even if the object plane is located at far field. While the field is demodulated achromatically (i.e. the spatial frequency of the output light

intensity distribution is zero), the phase of the output cosine function is wavelength dependent. Let us once again, limit the maximum misregistration to with 1/4 wave. That is,

$$\frac{Fd\alpha}{R}\left[\left(2+\lambda^2F^2+\frac{3F^4\lambda^4}{8}\right)-\left(2+(\lambda+\Delta\lambda)^2F^2+\frac{3F^4(\lambda+\Delta\lambda)^4}{8}\right)\right]\leq\frac{1}{4} \tag{29}$$

Then, the spectral bandwidth of the system must be limited to

$$\Delta\lambda_2 = R/4\alpha Fd(2\lambda F^2+\frac{3}{2}F^4\lambda^3) \tag{30}$$

For an on-axis point source ($\alpha = 0$), the system is completely achromatic. The system however, must remain achromatic for all points within the FOV. For a synthetic aperture imaging system, the FOV is defined by the footprint of the real aperture. Thus, the worst case represents $\alpha = R\lambda/A$. And since $d = \Delta S(\lambda)/2 \tan[\theta(\lambda)]$ where $\Delta S(\lambda)$ is the shear distance and $\theta(\lambda)$ is the diffraction angle for the center wavelength λ, the spectral bandwidth can be rewritten as

$$\Delta\lambda_2 = A\lambda/2\Delta s(\lambda)\cos\theta(\lambda)\left\{2[\sin^2\theta(\lambda)]/\lambda+3[\sin^4\theta(\lambda)]/2\lambda\right\} \tag{31}$$

We see that the achromatic spectral bandwidth is highly dependent on the diffraction angle θ (or equivalently, the spatial frequency of the gratings). To increase the achromatic bandwidth, θ must be made small. However, reducing the diffraction angle will increase the overall size of the interferometer. The light waves from the two input apertures have to travel a longer distance before they overlap. Thus, the optimum spatial frequency for the gratings in the

interferometer is one that provides an achromatic bandwidth that is just sufficient for the system operation.

Since the range of shear distances is limited by the system geometry to $\Delta\lambda_1 = 2A\lambda/S$, the grating interferometer only has to be achromatic over $\Delta\lambda_1$. The optimum spatial frequency for the gratings in the interferometer can be obtained by making the third order achromatic bandwidth in Eq. 31 equal to the desired achromatic bandwidth in Eq. 25. The two spectral bandwidths are equal when

$$4 \cos \theta(\lambda) \left[\frac{2 \sin^2 \theta(\lambda)}{\lambda} + \frac{3}{2} \frac{\sin^4 \theta(\lambda)}{\lambda} \right] = 1 \qquad (32)$$

or $\theta(\lambda) = 20.5^\circ$. For a center wavelength of $\lambda = 0.55$ μm, the optimum spatial frequency for the gratings will be

$$\frac{\sin \theta(\lambda)}{\lambda} = 700 \text{ lp/mm}.$$

If a FOV larger than $2R\lambda/A$ is desired (a larger FOV can be achieved by simply using a larger detector since the FOV is defined by $P * W_d$ where P is the point spread function of the real aperture projected out to the object plane, W_d is the width of the photo detector and * denotes convolution, then a lower spatial frequency F must be used to maintain the achromatic property over the entire FOV.

VI. APERTURE FILL

For a given interferometer geometry, the correlation output provides the value of the object spectrum at a single spatial frequency. The system geometry must be changed to generate transform data at other spatial frequencies in order to synthesize a two-dimensional aperture. First, if there is relative rotational motion about the optical axis between the object scene and the interferometer, transform data can be gathered along a circular arc in the transform plane. Second, if either the baseline or the detection wavelength is varied, transform data along a radial line in the transform plane is obtained. Combining these two effects, a two-dimensional aperture can be synthesized. The means to achieve such an aperture fill will be discussed below.

Let us assume for now that the interferometer is looking straight down at the object scene located at the optical axis. The interferometer output provides the transform data at a single point in the Fourier transform plane. As the object (or equivalently, the interferometer) rotates about the optical axis, data is gathered along a circular arc. To see what the phase history will look like as the target rotates relative to the sensor, consider a single point target located at a distance α_0 from the optical axis. Its Fourier spectrum is a linear phase in the x-direction and the in-phase or quadrature portion of the Fourier spectrum is a sinusoidal pattern with spatial frequency of approximately $\alpha_0/R\lambda$. The interferometer

measures the Fourier spectrum of the object scene at spatial frequency $u = s/R\lambda = 2Fd/R$, $v = 0$. As the target or the interferometer rotates, the cosine/sine transforms of the object spectrum is at $u = \cos(\theta)\, s/R\lambda$ and $v = \sin(\theta)\, s/R\lambda$ are measured where θ is the angle of rotation. The correlation output of the interferometric sensor as a function of time (phase history) can be written as

$$I_o(\alpha_o, \Phi, t) = 1 + \cos\left\{\frac{4\pi \sin\left(\tan^{-1}(S/2R)\right)\, \alpha_o[1 - \cos(\omega t - \Phi)]}{\lambda_o}\right\} \tag{33}$$

which can be rewritten as

$$I_o(\alpha_o, \Phi, t) = 1 + \cos\left\{k\alpha_o[1 - \cos(\omega t - \Phi)]\right\} \tag{34}$$

where Φ is the angular position of the point target relative to the α axis, ω is the angular rotation rate and k is a constant.

In Figure 5, we show the correlation output as a function of time for point targets located at different positions (α_o, Φ) in the object scene as the object is rotated relative to the interferometer at a constant rate. Since an incoherent input scene can be considered as an superposition of incoherent point radiators, the correlation output for an extended source as the object rotates can be expressed as

$$I_o(t) = \sum_{n=1}^{N} \left\{1 + \cos\left[k\alpha_n\left(1 - \cos(\omega t - \Phi_n)\right)\right]\right\} \tag{35}$$

Radial fill of the synthetic aperture can be achieved with the use of baseline diversity or wavelength diversity. Since the spatial frequency measured is determined by $S/R\lambda$, it can be changed by varying S, the separation of the detection aperture (baseline) or λ, the detection wavelength. Baseline diversity can be accomplished with the grating interferometer by moving the three gratings closer or apart as shown in Figure 6. However, it may not the desired mode of operation for synthetic aperture imaging since it requires the use of large input windows to accomodate the change in baseline. It is often more preferrable to keep the input aperture fixed and achieve the radial aperture via the use of wavelength diversity. On the surface, it may seem that the use of wavelength diversity with an achromatic system is contradictory. We note however, that the interferometer has a finite instantaneous bandwidth and the whole band can be slid back and forth to obtain the wavelength diversity for radial aperture fill. This is accomplished by changing d, the separation between gratings G1-G2 and G3. Recall from Eq. 21 that the spatial frequency measured by the interferometer is equal to $2Fd/R$. Changing d thus varies the spatial frequency measured. It can be seen from Figure 7 that changing d is also equivalent to changing the center wavelength of measurement λ. The instantaneous achromatic bandwidth remains $2A\lambda/S$ for any d. The factor of 8 gain in SNR is maintained over the entire synthetic aperture.

For a single point source located at (α_0, β), varying d at a constant rate will generate a correlation output of

$$I_o(\alpha_o, \Phi, t) = 1 + \cos\left(\frac{k'\alpha_o Tt}{\cos\Phi}\right) \qquad (36)$$

where T is the linear translation rate of grating G3 and k' is a constant. The correlation output as a function of time is a sinusoid whose frequency is dependent on the position of the point source (α_o, Φ).

The two means of aperture (circular and radial) fill can be used together to generate a two-dimensional aperture. Unlike tomographic imaging, synthetic aperture imaging systems generally gather transform data over an angular range much less than 90 degrees and the two-dimensional aperture synthesized is typically a segment of the an annulus as shown in Figure 8. The image (half-power) resolution in the ground plane is approximately equal to

$$\rho_\alpha \cong \frac{R\lambda}{A_u} = \frac{R\lambda^2}{S\Delta\lambda}$$

$$\rho_\beta \cong \frac{R\lambda}{A_v} = \frac{R\lambda}{2\,S\,\sin\left(\frac{\Delta\theta}{2}\right)} \qquad (37)$$

where $\Delta\theta$ is the angle of rotation. The resolution in the α direction is proportional to λ^2 instead of λ because the size of the synthetic aperture is proportional to $\Delta\lambda/\lambda$. The aperture is larger for smaller λ if $\Delta\lambda$ is fixed. For example, a real aperture imaging system operating at 0.5 μm with a 10 cm aperture can achieve a ground plane resolution of 5 m x 5 m at a range of 1000 Km. A passive synthetic aperture imaging system with the same real aperture size and

an aperture separation of 2 m on the other hand, can achieve a ground plane resolution of 0.63 m x 0.58 m at the same distance with $\lambda = 0.5$ μm, $\Delta\lambda = 0.2$ μm, and $\Delta\theta = 25°$.

To synthesize a two-dimensional aperture using the grating interferometric sensor, there are two possible approaches that can be taken. First, the grating G3 can be dithered back and forth along the optical axis (changing d) as the target rotates. This creates a two-dimensional synthetic aperture that is continuous in the radial direction as shown in Figure 9(a). Alternately, multiple demodulation gratings (G_3) placed at different positions along the z-axis of the interferometer can be used to measure several spatial frequencies simultaneously. As the object scene rotates, an aperture composed of continuous arcs is obtained as illustrated in Figure 9(b). The advantage offered by the former approach is that only a single demodulation grating and detector is required. However, in some operating modes where the time available for data acquisition is restricted, it may not be feasible to dither the the grating fast enough to synthesize an acceptable aperture. The latter method gather multiple transform data simultaneously. Its drawback is the need for multiple sets of hardware such as gratings, detectors, amplifiers etc. The approach of choice will be dependent on the operating requirements of the particular application.

VII. IMPULSE RESPONSE

In the above formation for image resolution, the synthesized aperture was for simplicity assumed to be completely filled and has rectangular dimensions of A_u, and A_v. However, the synthesized aperture is likely to be a segment of an annulus and it is continuously filled along either radial lines or circular arcs. For a single point target, the shape of the impulse response (IPR) may not be important; the main concern is the width of the IPR which defines image resolution. In the imaging of an extended object however, the shape of the IPR (sidelobe structure) plays a vital role in the image quality. In this section, we examine what the impulse responses look like with different aperture fills. As described in the last section, a two-dimensional aperture can be synthesized by: (1) dithering the grating G3 along the optical axis of the interferometer or, (2) using multiple demodulation gratings placed at different positions along the optical axis. The first approach produces continuous radial fill and the later approach produces continuous circular arcs.

First, we show in Figure 10, the transform of a single radial line obtained by translating linearly the grating G3 along the optical axis while the object is stationary. Without object or interferometer rotation, high image resolution is obtained only along the α direction through the use of wavelength diversity. If there is object rotation, then a two-dimensional synthetic aperture can be generated by dithering the grating G3 back and forth along the

optical axis of the interferometer. The aperture fill obtained by dittering the grating is shown in Figure 11a and the resulting impulse response is given in Figure 11b. (The synthetic aperture used to obtain Figure 11b contained 25 radials lines. Much fewer lines are shown in Figure 11a in order to illustrate the structure more clearly.)

If the position of the grating is fixed, then a circular arc of transform data as shown in Figure 12a is obtained by rotating the object or the sensor. The bow tie-like impulse response of such an aperture is shown in Figure 12b. For this case, high image resolution is obtained in the β direction where a large aperture is synthesized through the rotating motion of the object or the sensor. By using multiple sets of gratings and detectors, a two-dimensional aperture fill as shown in Figure 13a is obtained. The corresponding impulse response of a synthetic aperture containing 25 arcs is given in Figure 13b. The impulse responses obtained with the two approaches for aperture fill are different in fine structures but their over all image qualities are about equivalent. We may note also that the two approaches can be combined. A small set of grating/detectors may be used to obtain simultaneous measurements of several spatial frequencies and the gratings may also be dithered together to fill in the gaps. Combining the two approaches would reduce the number of grating/detector sets required and decrease the amount of grating travel needed to fill the desired aperture when

compared to systems utilizing either approach alone. The minimum spacing required between transform data is dependent on the size of the FOV. Further the target is from the scene center (optical axis), steeper is the linear phase at the transform or detection plane. In practice, one would like to have at least two and preferrably four samples per cycle. This sampling requirement dictates the speed with which the grating is dit ered in the first approach and the spacings of the d modulation gratings in the second approach.

VIII. EXPERIMENTS

A grating interferometer was set up in the laboratory and experiments were performed to demonstrate some of the concepts described above. It is difficult to perform optical synthetic aperture imaging experiments in the laboratory because of the problems posed by the short target range that is available. First of all, the grating interferometric sensor requires the far field condition to be satisfied between the object and detection planes. Moreover, image resolution at optical wavelengths at such short ranges are very high. This would require the use of either a very small sensor or a very small target scene.

The gratings we used in the experiments were fabricated on dichromated gelatin using two plane waves in a symmetric geometry to produce a spatial frequency of 500 lp/mm. Ideally, grating G1 and G2 should be fabricated with an asymmetric geometry such that diffraction favors a single order while the grating G3 should be fabricated with a symmetric recording geometry to produce two (±1) orders of equal intensity. However, to ensure that all the gratings have identical spatial frequency, the same recording geometry was used for all the gratings.

The experiment was performed on a 4' x 8' optical bench. It provided a target range of about 1.5 m. In order for the FOV to be of workable size, a real collection aperture of 0.5 mm was used. The

size of the corresponding point spread function at the object plane was 1.5 mm. The apertures were separated by 10 mm, giving a A/S ratio of 1:20. Since the aperture separation is so small, gratings G1 and G2 were implemented by masking off a single grating instead of using two individual gratings. To simulate the far field condition at such a short target range, an achromatic lens with a focal length of 1.5 m is placed in front of the grating as shown in Figure 14 to collimate the incoming field. To study the responses of the grating interferometer and compare it with theory, a rotating wide-band point source was generated by rotating a pinhole that is back illuminated by an unfiltered Xenon arc lamp. To be a "point" source to the sensor, the size of the source must be smaller than the period of the spatial frequency being measured. For the system geometry used in the experiment, it means that the source diameter must be less than 75 μm. A 25 μm pin hole was used in our experiments. Grating G3 was placed at an nominal distance of 17.5 mm from G1-G2 and it was mounted on a stepping motor driven linear translation stage in the Z direction and a piezoelectric driven translator in the x direction. The output light field was focussed on a fiber optics probe and detected by a photomultiplier. The output intensity was then digitized and transferred to a computer.

In Figure 15a, we show the sensor output with the geometry of the grating interferometer fixed and the point source rotating over an angular range of ±45°. It is identical to the phase history

described by Eq. 34 and presented in Figure 5. The grating G3 was then translated by 1/8 of a fringe producing a $\pm\pi/4$ phase shifts on the recombined fields. The quadrature data was obtained as shown in Figure 15b.

To observe the ability of the system to resolve images in the β direction with the use of object rotation to build a synthetic aperture, the point source was placed at a starting position as shown in Figure 16a and the output is compressed to form a point image in the β direction. In Figure 16b, we show the ideal theoretical sensor output and in Figure 16c, the experimentally obtained data. The corresponding compressed image is shown in Figure 16d. Next, the starting point of the rotator point source was retarded to simulate a second point target off-set along a circular arc as shown in Figure 16e. The sensor output is given in Figure 16g and the compressed image in Figure 16h. We see that the compressed image is off-set accordingly.

To observe image compression in the x direction using wavelength diversity to generate the synthetic aperture, the grating G3 was translated at an uniform rate while the point target was kept stationary. In Figure 17a, we show the position of the point source and in Figure 17b, the sensor output. It is a sinusoidal pattern as described in Eq. 36. The compressed image is shown in Figure 17c. The point source is then moved closer to the optical center and the resulting sensor output is shown in Figure 17d and the corresponding

compressed image is given in Figure 17e. Once again, the difference in the location of the two point sources along the α direction is resolved.

The experiments performed were simple, demonstrating separately aperture synthesis along the two dimensions using object rotation and wavelength diversity. Nevertheless, the experimental results demonstrate very well the feasibility of using an achromatic grating interferometer for passive synthetic aperture imaging of spectrally wide band object scenes. Work is continuing toward the demonstration of passive synthetic aperture imaging of two-dimensional extended objects.

IX. COMPARISON WITH CONVENTIONAL INTERFEROMETERS

We have shown in Section V that a subtantially wider instantaneous spectral bandwidth can be used with the grating interferometer than with a conventional interferometer, thereby giving the grating interferometer better sensitivity. There are also operational advantages in using the grating interferometer. In a conventional system, the measurement wavelengths and thus the spatial frequencies, are selected with a bank of narrow band spectral filters. With the grating interferometer on the other hand, it is determined by the position of the gratings which can be varied continuously. Therefore, continuous radial fill is difficult to achieve with conventional interferometers (without changing the baseline) but simple to implement with a grating interferometer. Due to the sampling requirements, measurement at many wavelengths is often required to generate an adequate aperture fill. The number of parallel channels required could be fairly large (>30). The grating interferometer provides the option of using a single or a small number of parallel channels. The aperture fill is obtained by simply dithering a single or a small set of gratings.

The grating interferometer is also less sensitive to system vibrationsand accurate phase shifts can be more easily achieved since the phases of a diffracted waves are determined mainly by the lateral position of the grating fringes. Moving a grating laterally by one fringe period (5 um) produces one full wave of phase

shift. It is therefore 10 times less sensitive to component motion than conventional interferometers that employ mirrors and beam splitters.

X. SUMMARY

In this paper, we have introduced the use of a grating interferometer for passive synthetic aperture imaging. Since natural emissions and illuminating sources are spectrally very wide band, the larger instantaneous spectral bandwidth permitted by the grating interferometer provides the grating based sensor with better system sensitivity than conventional systems. Moreover, the grating interferometer provides a simple means to achieve radial aperture fill through the use of wavelength diversity and the interferometer is more tolerant to system vibration. Possible operating modes that can be used to generate two-dimensional synthetic apertures were presented and the resulting impulse responses were compared. Simple experiments were performed to demonstrate the concepts proposed and the results were consistent with theories.

The author gratefully acknowledges the valuable contributions of I. LaHaie, K. Ellis, I. Cindrich and C. Aleksoff to this project. The work reported in this paper was supported by the U.S. Army Research Office.

References:

1) W.M. Brown and L.J. Porcello, "An introduction to synthetic aperture radar," IEEE Spectrum, Vol.6,p.52,1969.

2) W.M. Brown, "Synthetic Aperture Radar," IEEE Trans. Aerosp. Electron. Syst.,Vol.AES-3, p.217, 1967.

3) E.N. Leith, "Quasi-Holographic Techniques in the Microwave Region," Proc. IEEE, Vol.59, p.1305, 1971.

4) J.L. Walker, "Range-Doppler Imaging of Rotating Objects," IEEE Trans. Aerosp. Electron. Syst., Vol.AES-16, p.23, 1980.

5) C.C. Aleksoff, " Interferometric two-dimensional imaging of rotating objects," Opt. Lett. Vol.1,p.54,1977.

6) E.B. Fomalont, "Earth-Rotation Aperture Synthesis," Proc. IEEE, Vol. 61, p. 1211, 1973.

7) M. Born and E. Wolf, Principles of Optics, (MacMillan Co. New York, 1964), Chapter 8.

8) B.J. Chang and E. Leith,"Space-Invariant multiple-grating Interferometer in Holography," J. Opt. Soc. Am. Vol.69,p.689, 1979.

9) G.D. Collins,"Achromatic Fourier Transform Holography,"Appl. Opt. Vol.20, p.3109, 1981.

10) A. Tai et al, "Imaging through scattering media by Interferometric techniques," Appl. opt. 20, p.2484, 1981.

11) A. Tai and C. Aleksoff,"Grating-based interferometric processor for real time optical Fourier transformation," Appl. Opt. Vol.23, p.2282, 1984.

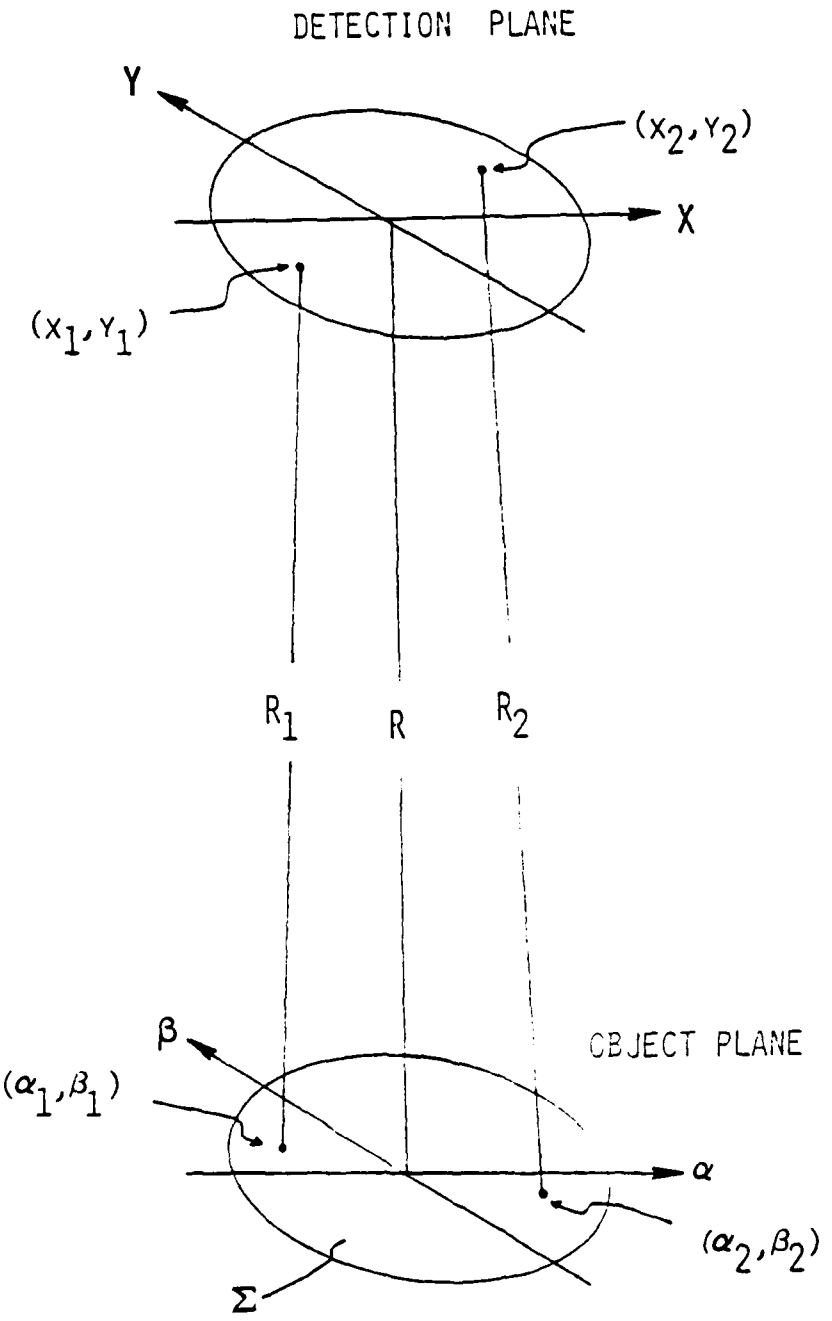

Figure 1: System Geometry for Passive Interferometric Imaging.

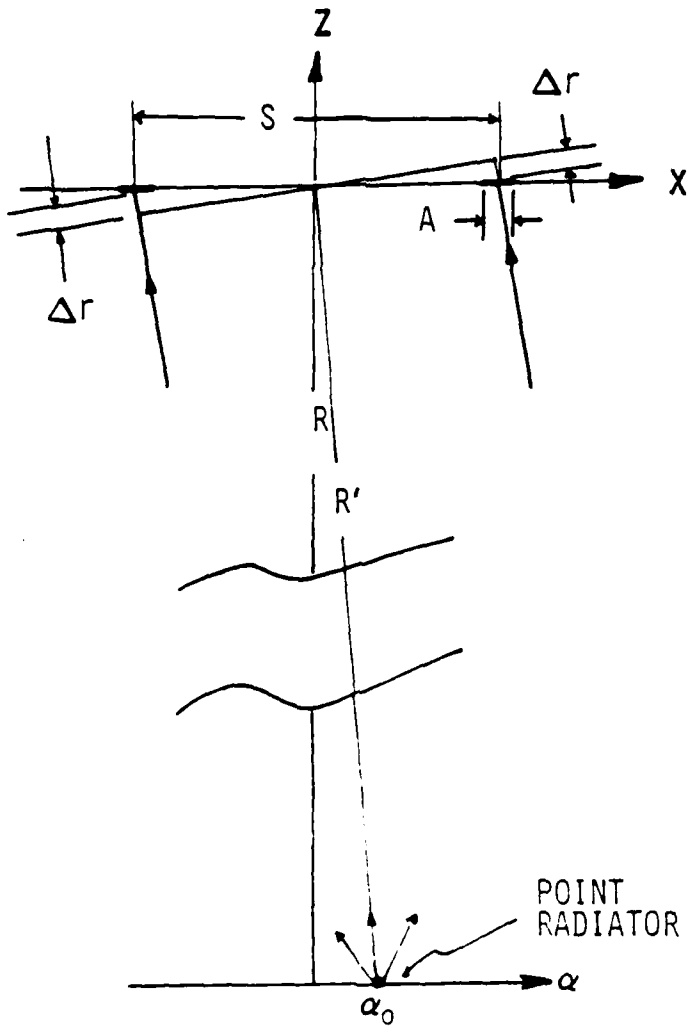

Figure 2: System Geometry for Correlation Measurements with a Conventional Interferometer.

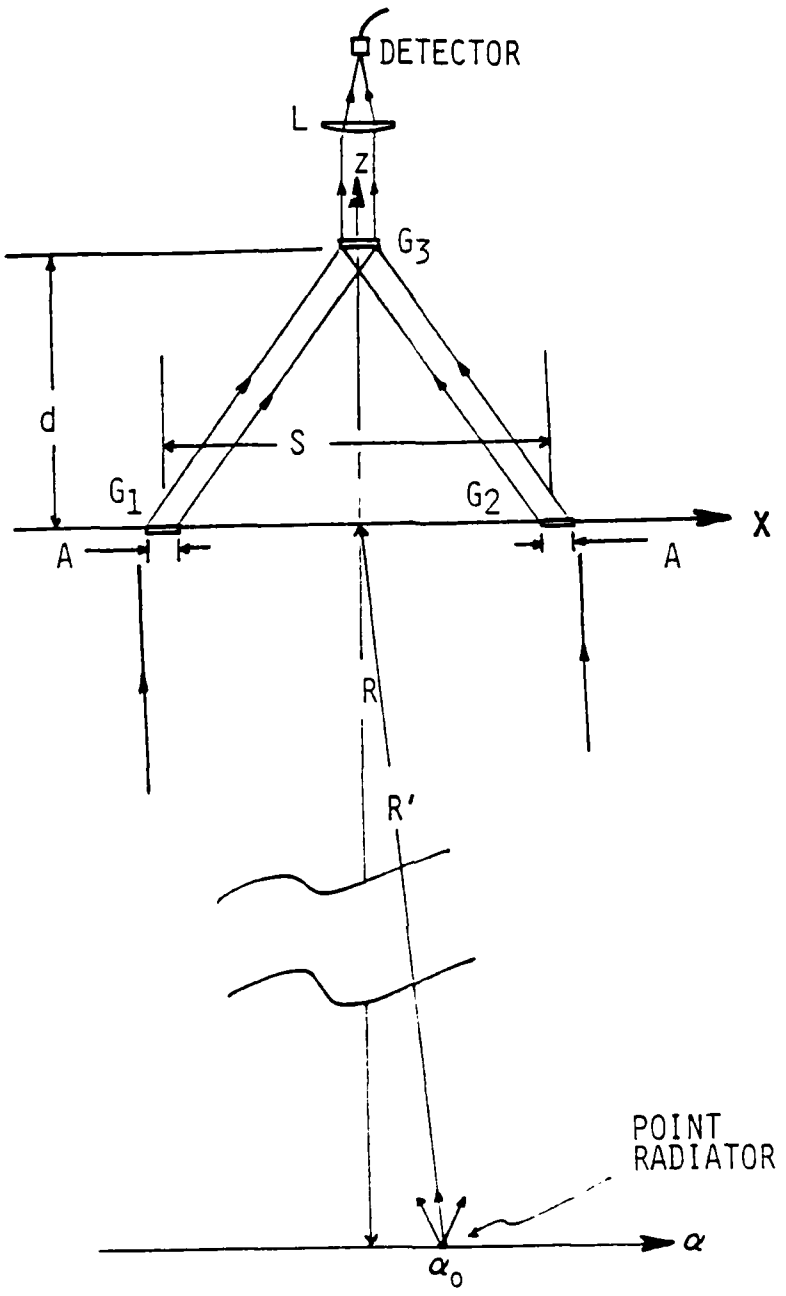

Figure 3: System Geometry for Passive Synthetic Aperture Imaging with a Grating Interferometer.

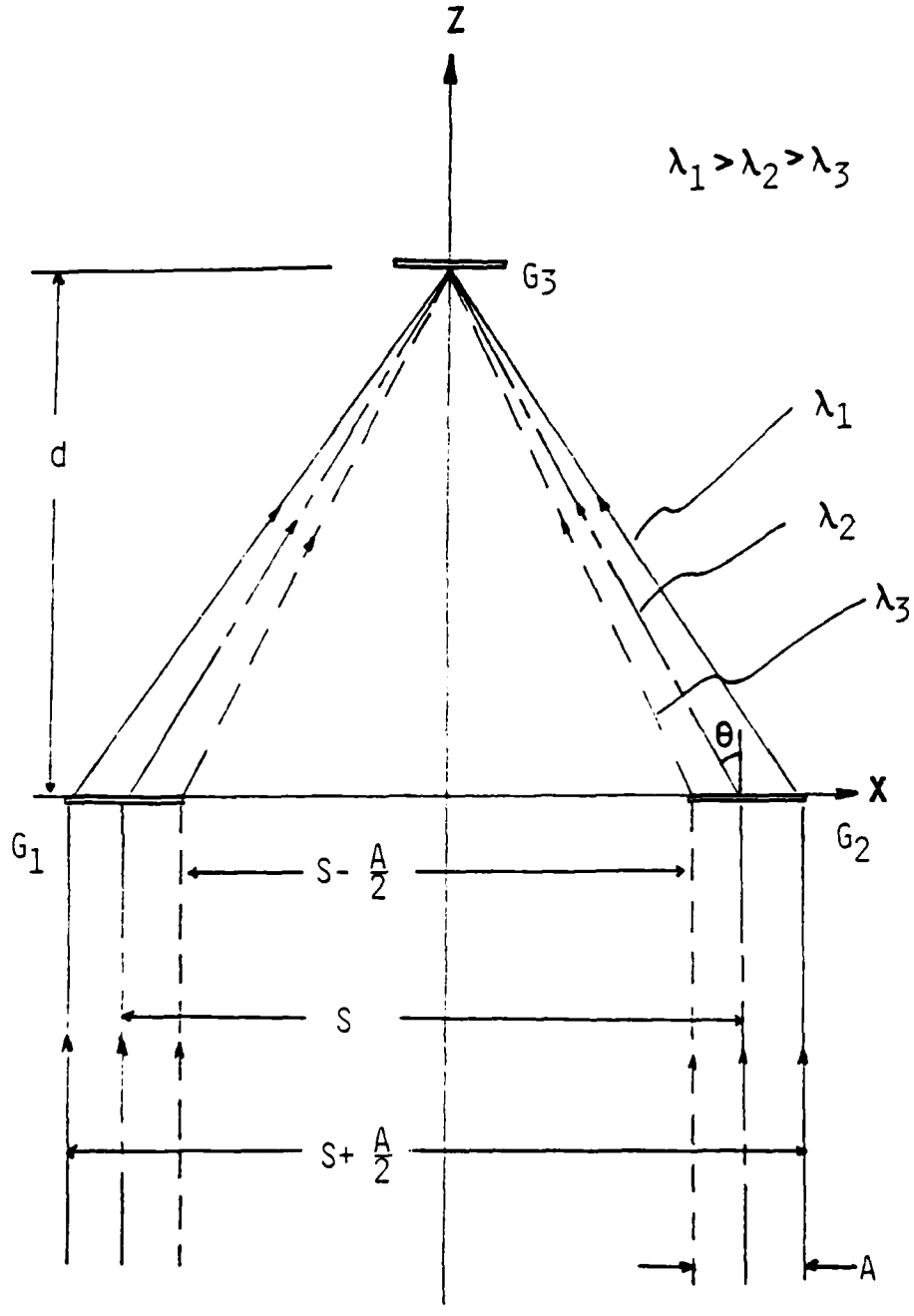

Figure 4: Wavelength Dependent lateral shear of the Field being Correlated.

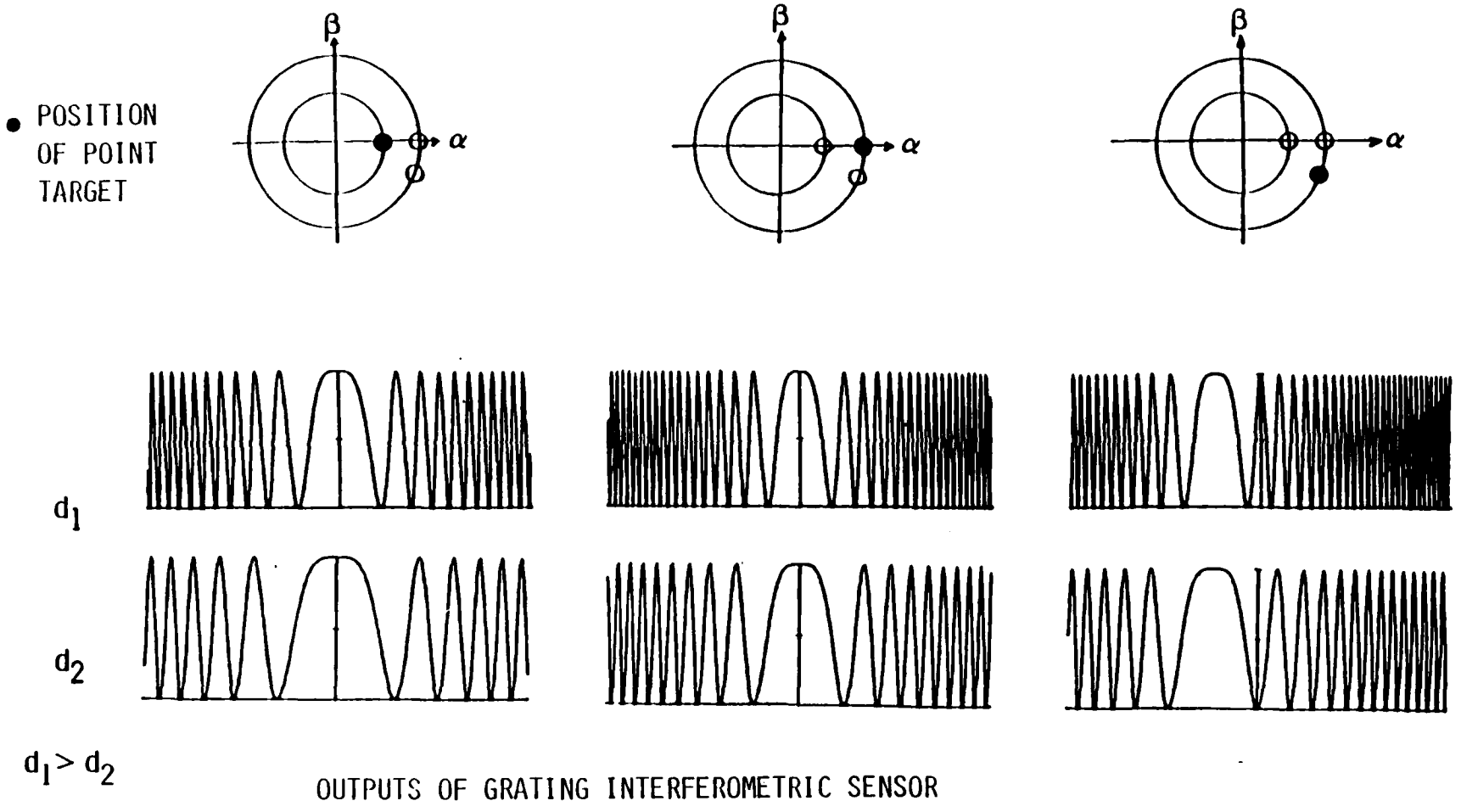

Figure 5: Theoretical Correlation Outputs Obtained with a Grating Interferometer as a function of the Target Position and the Spatial Frequency measured as defined by the position of Grating G_3.

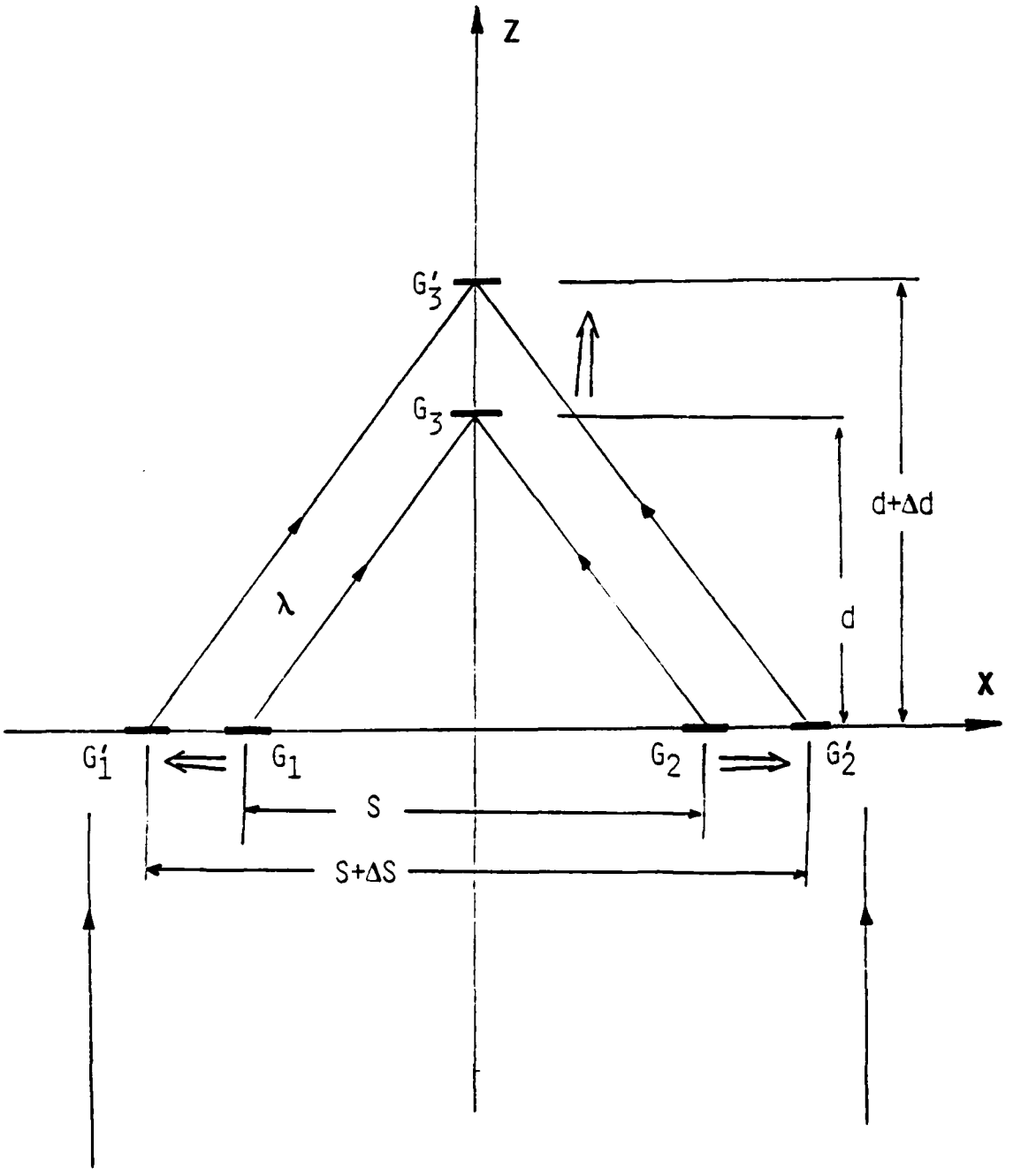

Figure 6: Implementation of Base-line Diversity by Moving the Gratings Closer or Farther Apart.

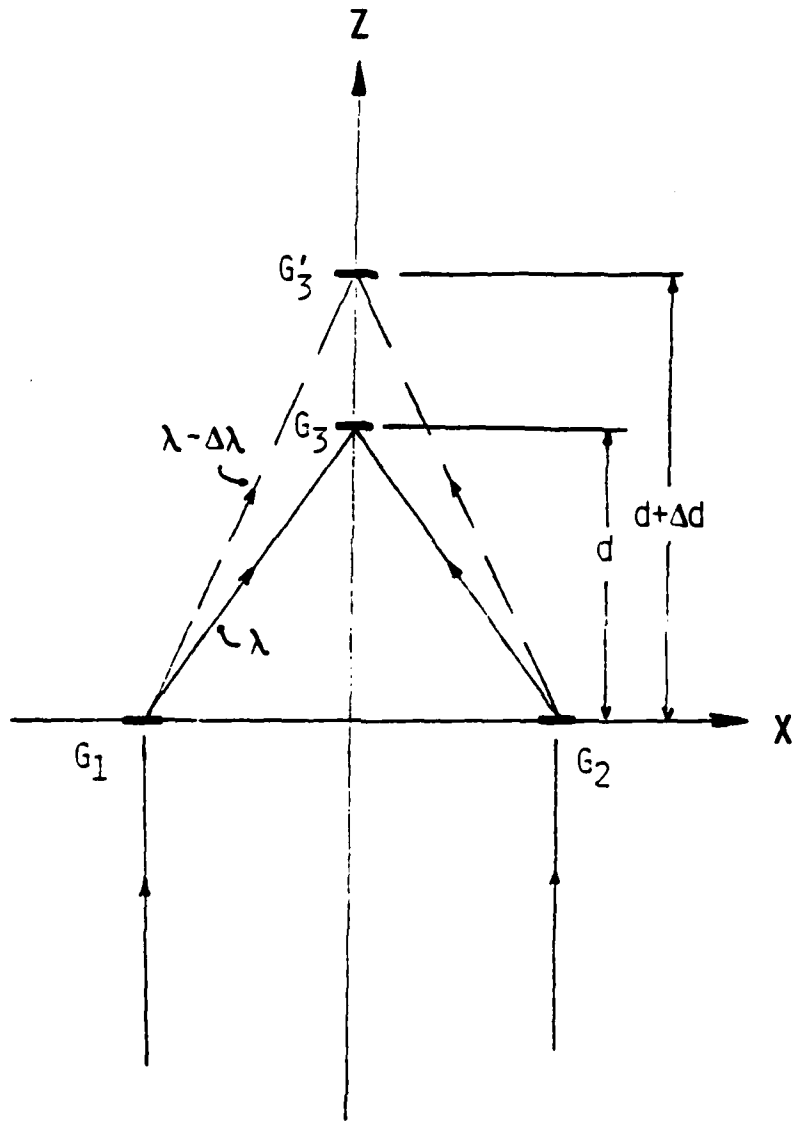

Figure 7 : Wavelength Diversity as Implemented by the translation of Grating G_3.

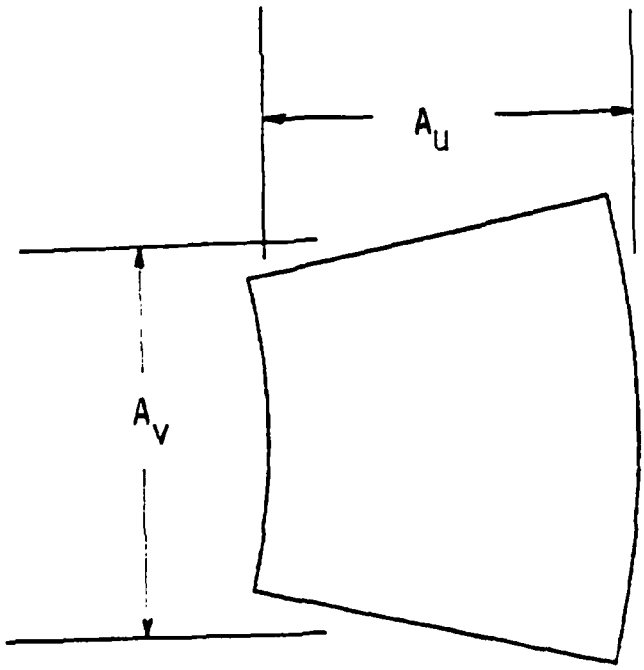

Figure 8: Band Pass Synthetic Aperture Generated by Object Rotation and Wavelength Diversity.

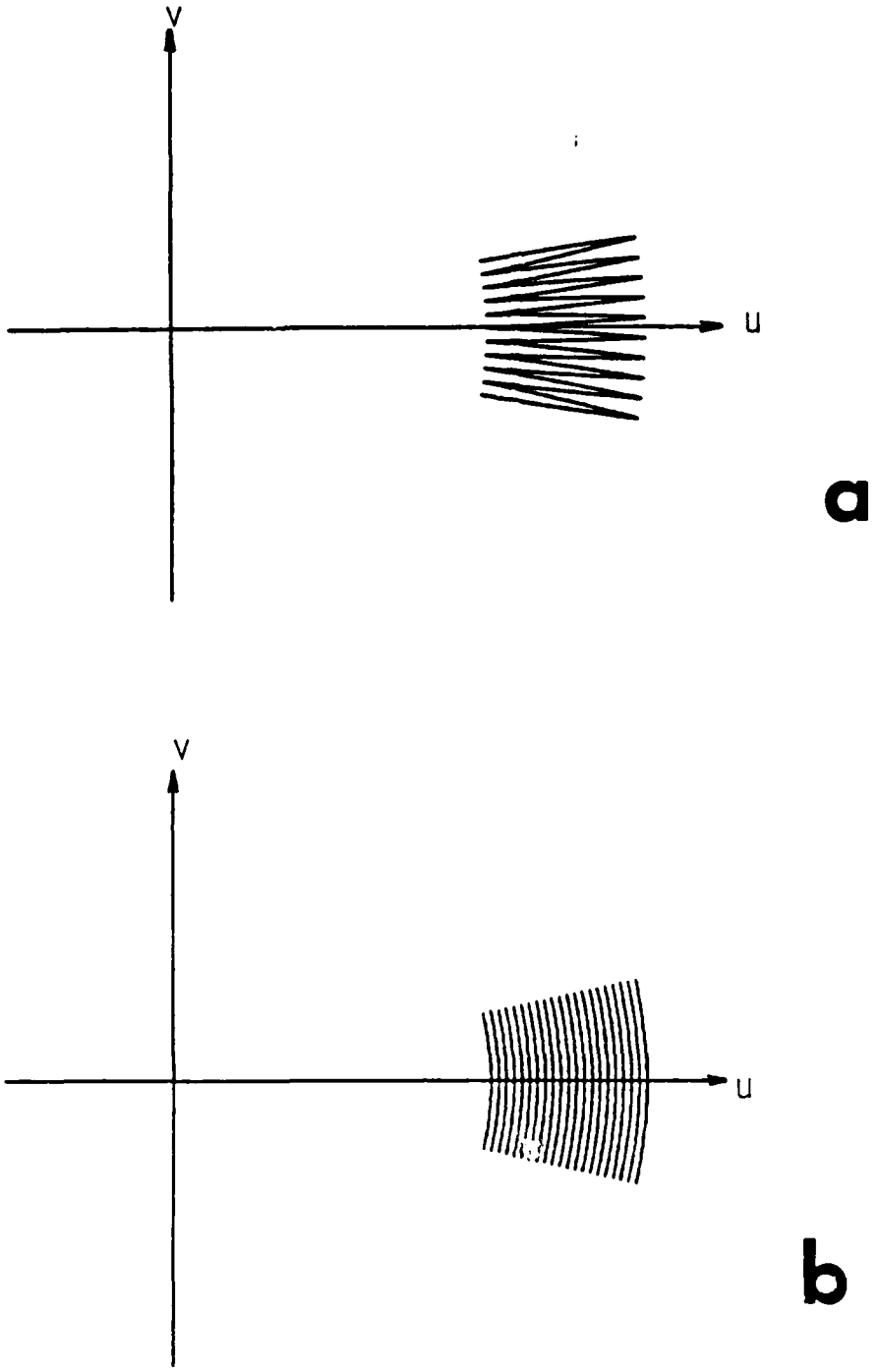

Figure 9: Synthetic Aperture Generated by a) dittering the grating G_3 while the object rotates, and b) utilizing multiple demodulation gratings.

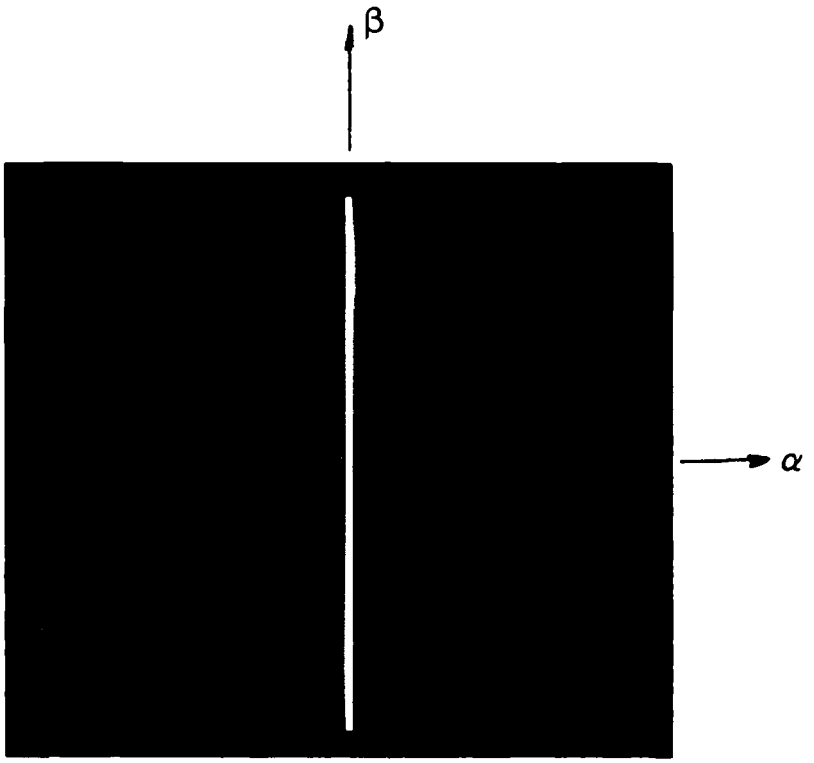

Figure 10: Reconstructed Image of a Point Target with a Single Radial Line of Transform Data.

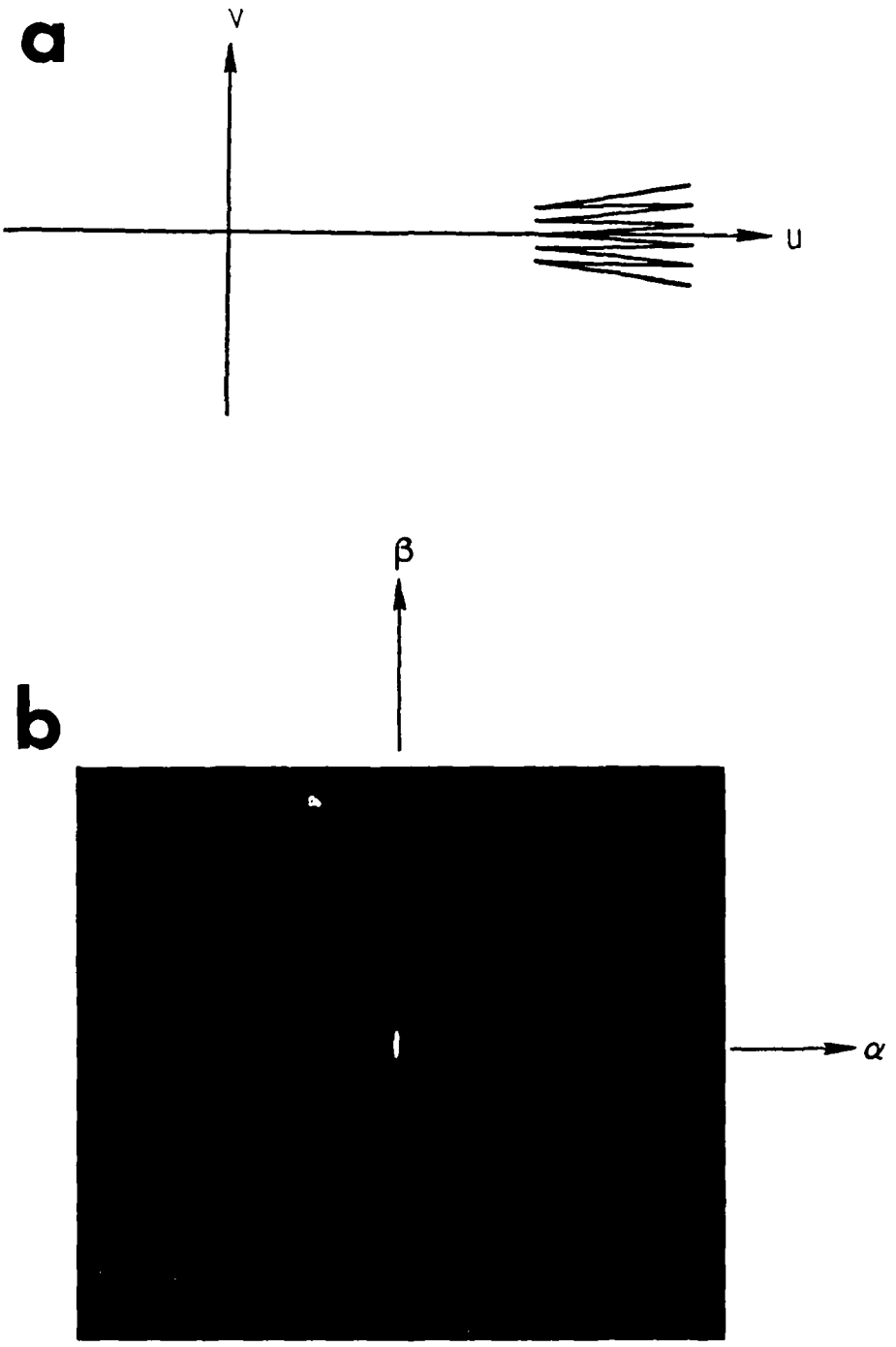

Figure 11: Impulse Reponse of a Synthetic Aperture Generated by Dittering Demodulation Grating G_3. a) Synthetic Aperture and b) Reconstructed Image of Point Target.

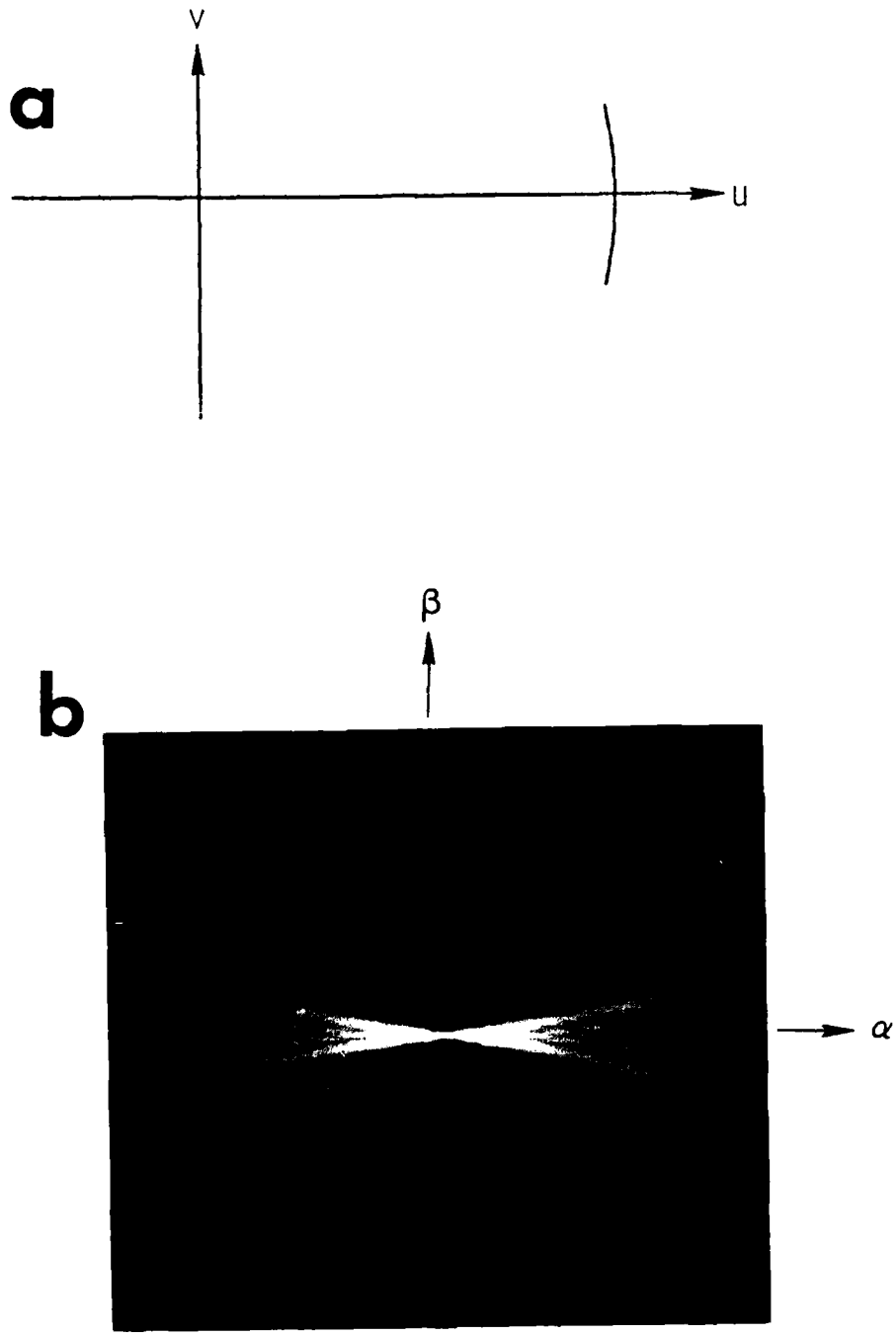

Figure 12: Impulse Response of a Single Arc of Transform Data. a) Synthetic Aperture and b) Reconstructed Image of a Point Target.

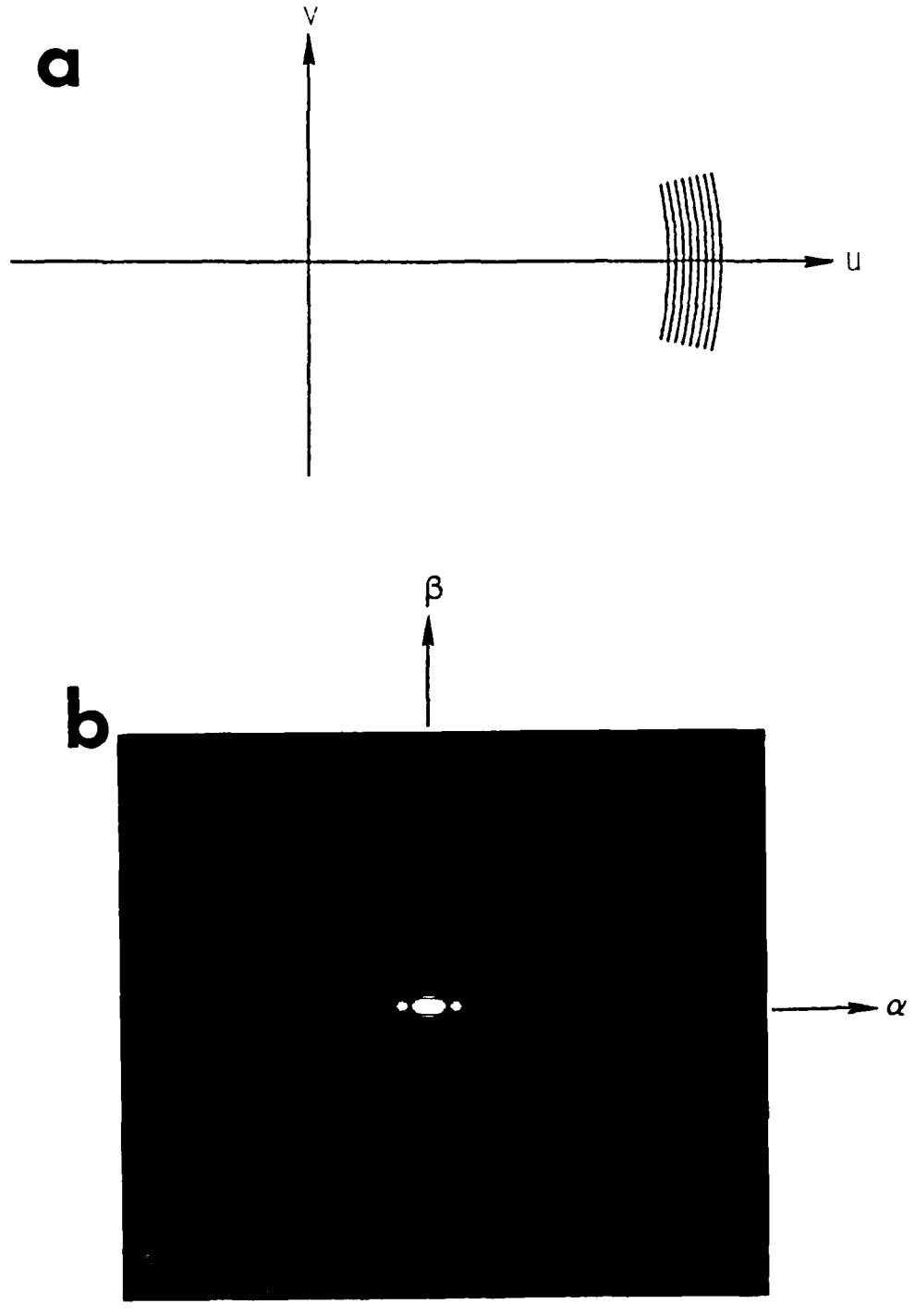

Figure 13: Impulse of a Synthetic Aperture Generated with Multiple Demodulation Gratings. a) Synthetic Aperture and b) Reconstructed Image of a Point Target.

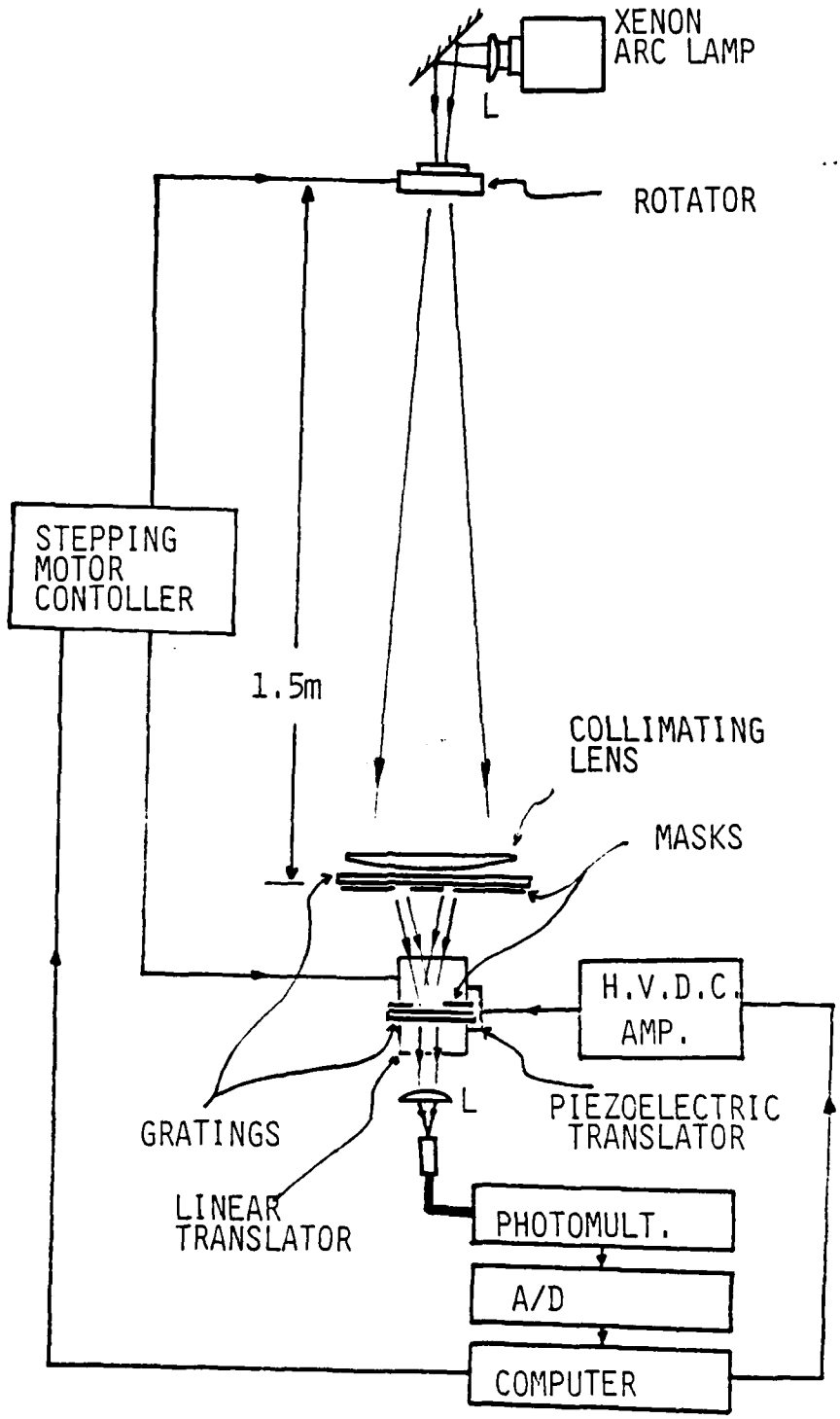

Figure 14: Experimental System for the demonstration of Passive Synthetic Aperture Imaging Concept.

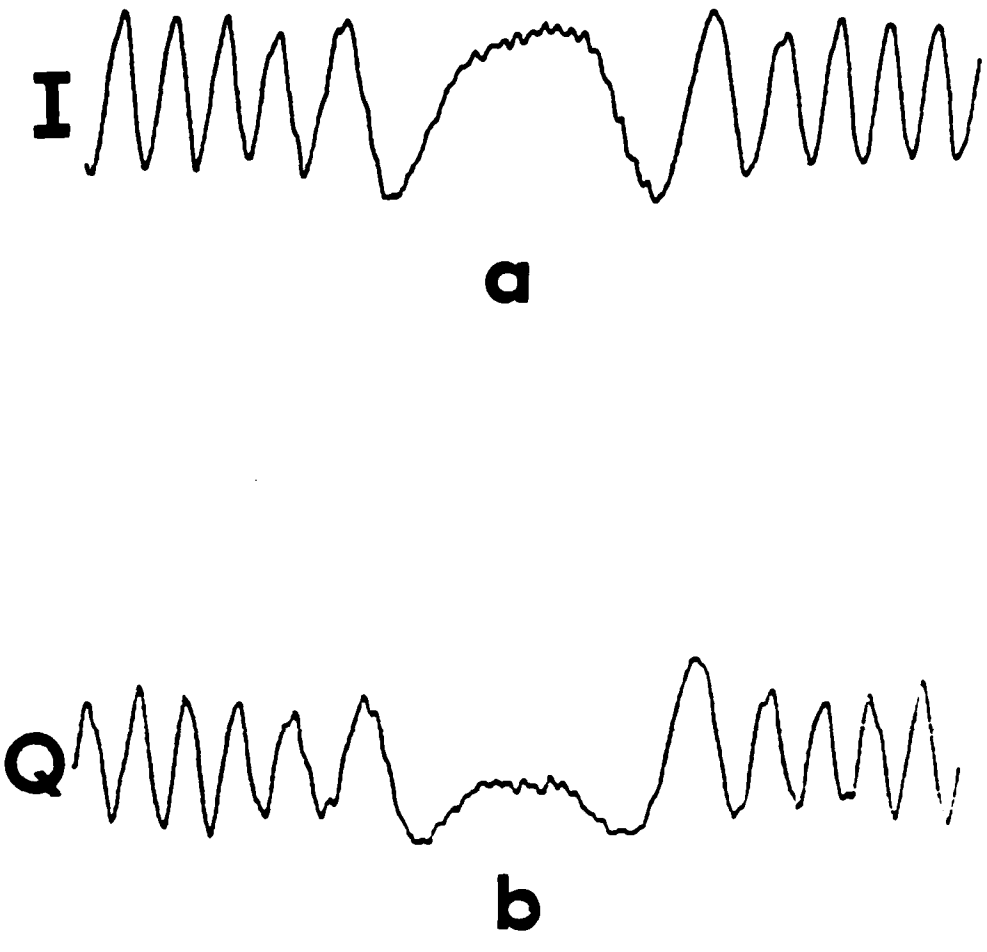

Figure 15: In-Phase and Quadrature Transform Data Obtained with a Grating Interferometer.

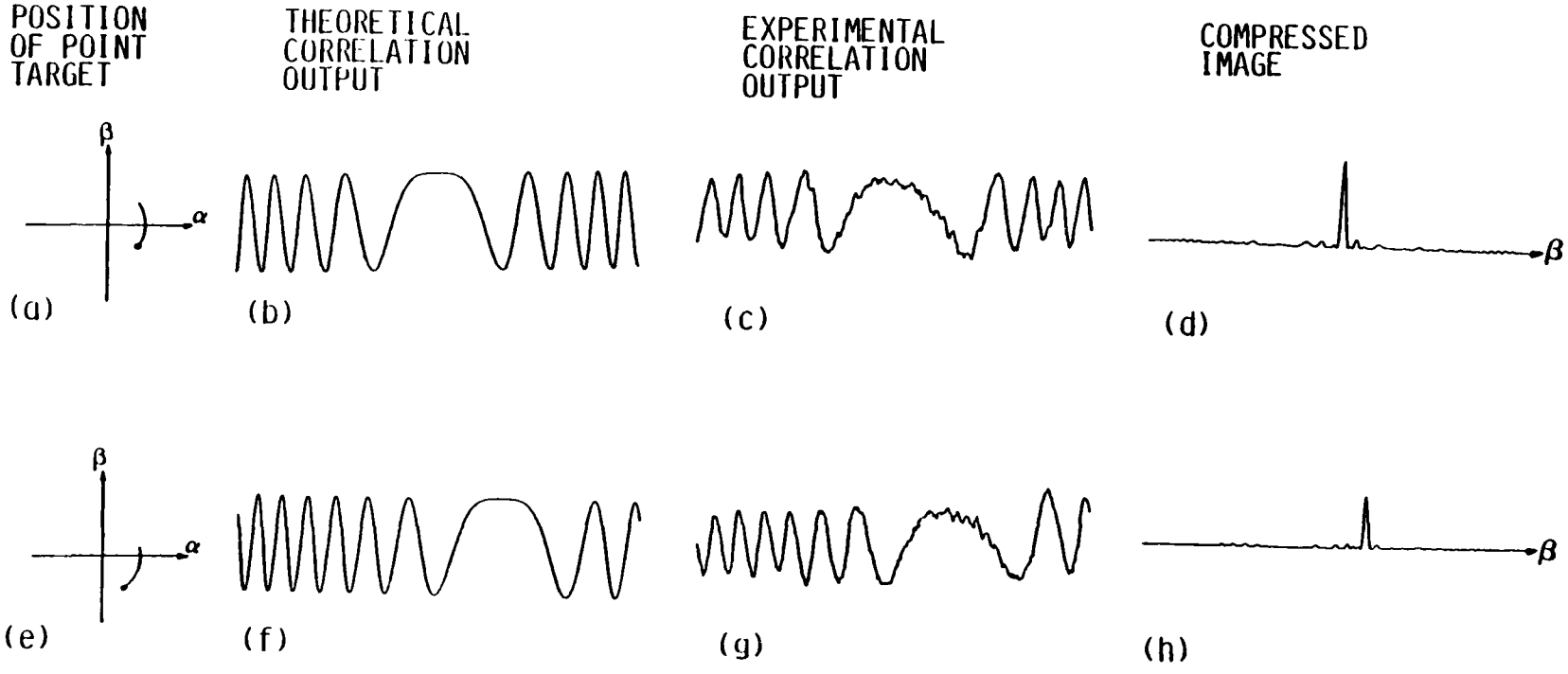

Figure 16: Experimental Results Demonstrating Image Compression in the β-Direction Using Object Rotation for Aperture Synthesis.

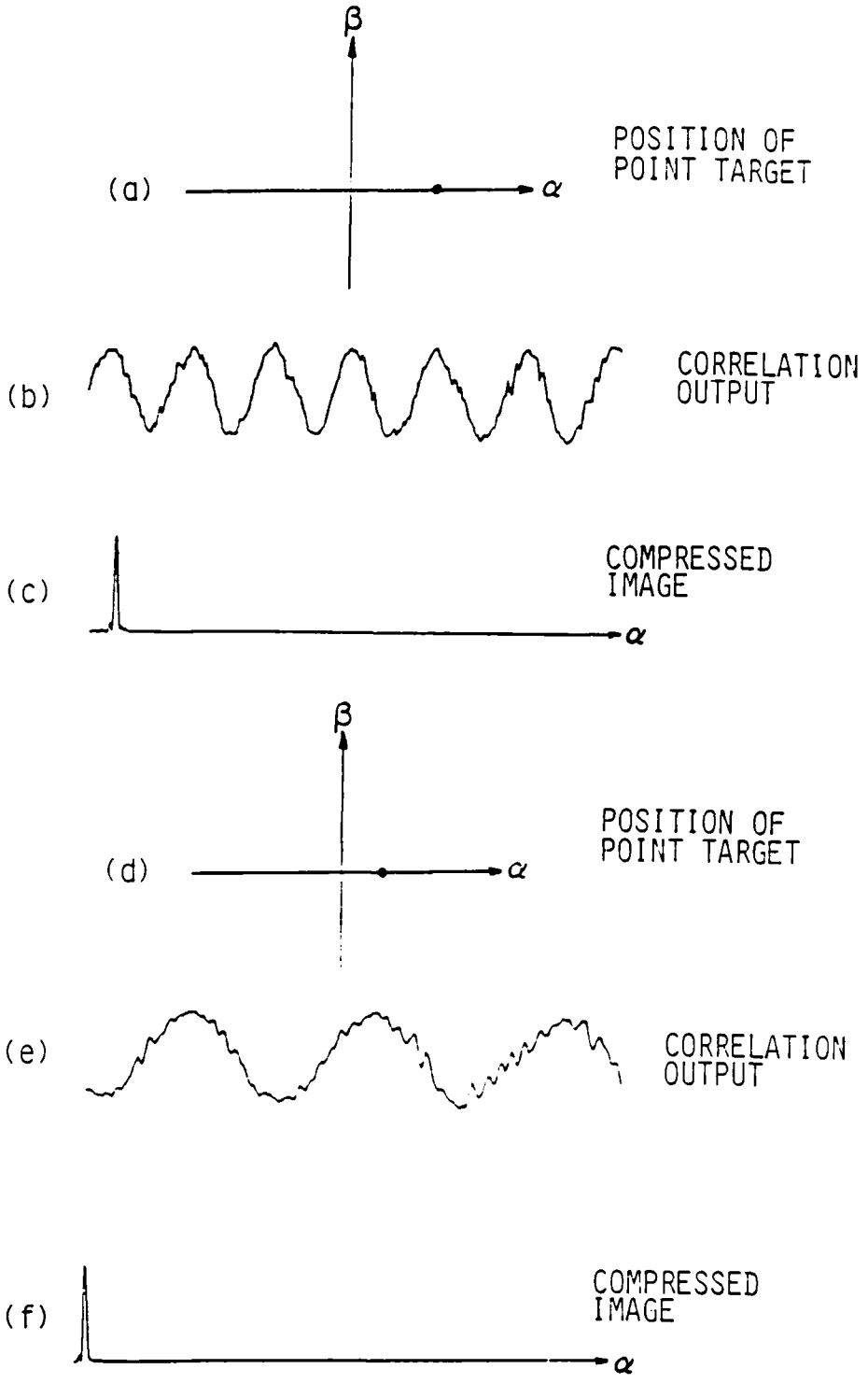

Figure 17: Experimental Results Demonstrating Image Compression in the α-Direction using Wavelength Diversity for Aperture Synthesis.

END
FILMED
4-86
DTIC